THE CONTENTNEA CREEK GRANITE: CONSTRAINTS ON LATE PALEOZOIC MAGMATISM AND DEFORMATION, EASTERN PIEDMONT FAULT SYSTEM, NORTH CAROLINA

By

Richard W. Burns

July, 2015

Director of Thesis: Eric Horsman

Major Department: Geological Sciences

The Alleghanian orogeny is manifested in eastern North Carolina by dextral transpressional faulting on the Eastern Piedmont Fault system and spatially associated granitic magmatism. The Contentnea Creek granite in Wilson County, North Carolina, is exposed over ~20 km^2 and is spatially associated with the Hollister mylonite zone, a component of the Eastern Piedmont Fault system. For this study, field observations and laboratory analyses are used to characterize fabric variation, geochemical signature, and the timing of the Contentnea Creek pluton, with the goal of understanding its place in the regional Alleghanian thermo-tectonic history. Multiple fabrics exist in the Contentnea Creek pluton. On the eastern margin of the pluton magmatic fabric exists. On the western margin of the pluton high-temperature solid-state fabric exists and preserves evidence of syn-magmatic shearing within the Hollister mylonite zone. The high-temperature solid-state fabric is locally overprinted by low-temperature solid-state fabric that formed in zones of high strain rates. Isolated clusters of mineralized shear fractures overprint both solid-state fabrics and likely formed much later, after these rocks were exhumed into the upper crust. Whole-rock major and trace element geochemical data demonstrate that the pluton is homogenous within the exposed area and is similar to other Alleghanian granitoids in the southern Appalachians. ID-TIMS U/Pb geochronology on zircon

yields a 305.70 ± 0.22 Ma crystallization age. These new data from the Contentnea Creek pluton refine our understanding of the spatial and temporal relationship between regional Alleghanian magmatism and faulting. Mineralized shear fractures overprint late Paleozoic Alleghanian structures after their exhumation into the upper crust. Paleostress analysis suggests late brittle fractures may have formed due to Cenozoic reactivation of the Eastern Piedmont Fault system, as has been observed elsewhere to the north and south, along the strike of this major late Paleozoic structure.

THE CONTENTNEA CREEK GRANITE: CONSTRAINTS ON LATE PALEOZOIC

MAGMATISM AND DEFORMATION, EASTERN PIEDMONT FAULT SYSTEM, NORTH

CAROLINA

A Thesis

Presented to the Faculty of the Department of Geological Sciences

East Carolina University

In Partial Fulfillment of the Requirements for the Degree

Master of Science in Geology

By

Richard W. Burns

July, 2015

THE CONTENTNEA CREEK GRANITE:

CONSTRAINTS ON LATE PALEOZOIC MAGMATISM AND DEFORMATION,

EASTERN PIEDMONT FAULT SYSTEM, NORTH CAROLINA

By

Richard W. Burns

APPROVED BY:

DIRECTOR OF THESIS:_____
Eric Horsman, PhD

COMMITTEE MEMBER:_____
Donald Neal, PhD

COMMITTEE MEMBER:_____
Adriana Heimann, PhD

COMMITTEE MEMBER:_____
Drew Coleman, PhD

CHAIR OF THE DEPARTMENT
OF GEOLOGICAL SCIENCES:_____
Stephen J. Culver, PhD

DEAN OF THE
GRADUATE SCHOOL:_____
Paul J. Gemperline, PhD

Table of Contents

List of Tables

List of Figures

List of Abbreviations

1. Introduction

Metamorphism, deformation, and magmatism associated with the Alleghanian orogeny occurred from ~330 to 250 Ma throughout the eastern Piedmont of North Carolina (Snoke et al., 1980; Farrar, 1985b; Russell et al., 1985; Speer et al., 1994). In the same region, dextral transpression associated with the Alleghanian orogeny produced the regional-scale Eastern Piedmont Fault system (EPFS) (Figure 1). The Hollister mylonite zone (HMZ) is the easternmost component of the EPFS and is the proposed eastern boundary of Alleghanian metamorphism and deformation in the region (Russell et al., 1985).

A close spatial relationship exists between Alleghanian plutons, the EPFS, and areas of regional Alleghanian metamorphism (Speer et al., 1994). Detailed studies of these intrusions have been vital in understanding the relationship between faulting and magmatism in the southern Appalachians, the eastern Piedmont of North Carolina (Snoke et al., 1980; Farrar, 1985b; Russell et al., 1985; Moncla, 1990; Speer et al., 1994), and elsewhere.

The Contentnea Creek pluton is an elliptical granitic body spatially associated with the EPFS in southern Wilson County, North Carolina. Available exposures and gravity data (Lawrence, 1999) suggest the intrusion is a northwest to southeast-elongated body bordered by the HMZ to the west. Geobarometry (Vyhnal and McSween, 1990) suggests other Alleghanian plutons in the region were emplaced in the mid crust. Away from the mylonite zone, the granitic body displays magmatic fabrics, while in areas affected by the mylonite zone it shows a high-temperature solid-state fabric consistent with emplacement in an active shear zone. Locally, the high-temperature solid-state fabric is overprinted by a low-temperature solid-state fabric and later mineralized shear fractures. The Contentnea Creek pluton thus contains evidence of both Alleghanian and later deformation.

The later mineralized shear fractures overprint mid-crustal fabrics and provide evidence of recent faulting. During the late Cenozoic, compressional stresses have dominated the eastern United States (Marple and Talwani, 2000). Reactivation of ancient fault systems and terrane boundaries has been documented in Virginia, South Carolina, and Georgia. Similar reactivation in North Carolina has been previously suggested (e.g. Prowell, 1983), but remains poorly studied.

This study explores the geochemical and structural characteristics of the Contentnea Creek pluton as well as its spatial and temporal relationship with the HMZ. Lab work included petrography, shape preferred orientation analysis, anisotropy of magnetic susceptibility analysis, whole-rock major and trace element geochemistry, U-Pb zircon geochronology, and paleostress analysis. The results from these methods allow me to (1) describe fabric variations that exist within the intrusion on a fault-perpendicular transect; (2) compare major and trace element geochemistry to other Alleghanian intrusions; (3) determine the age of the Contentnea Creek pluton and thereby place constraints on the ages of events which modified the intrusion and (4) constrain brittle deformation present in the Contentnea Creek pluton.
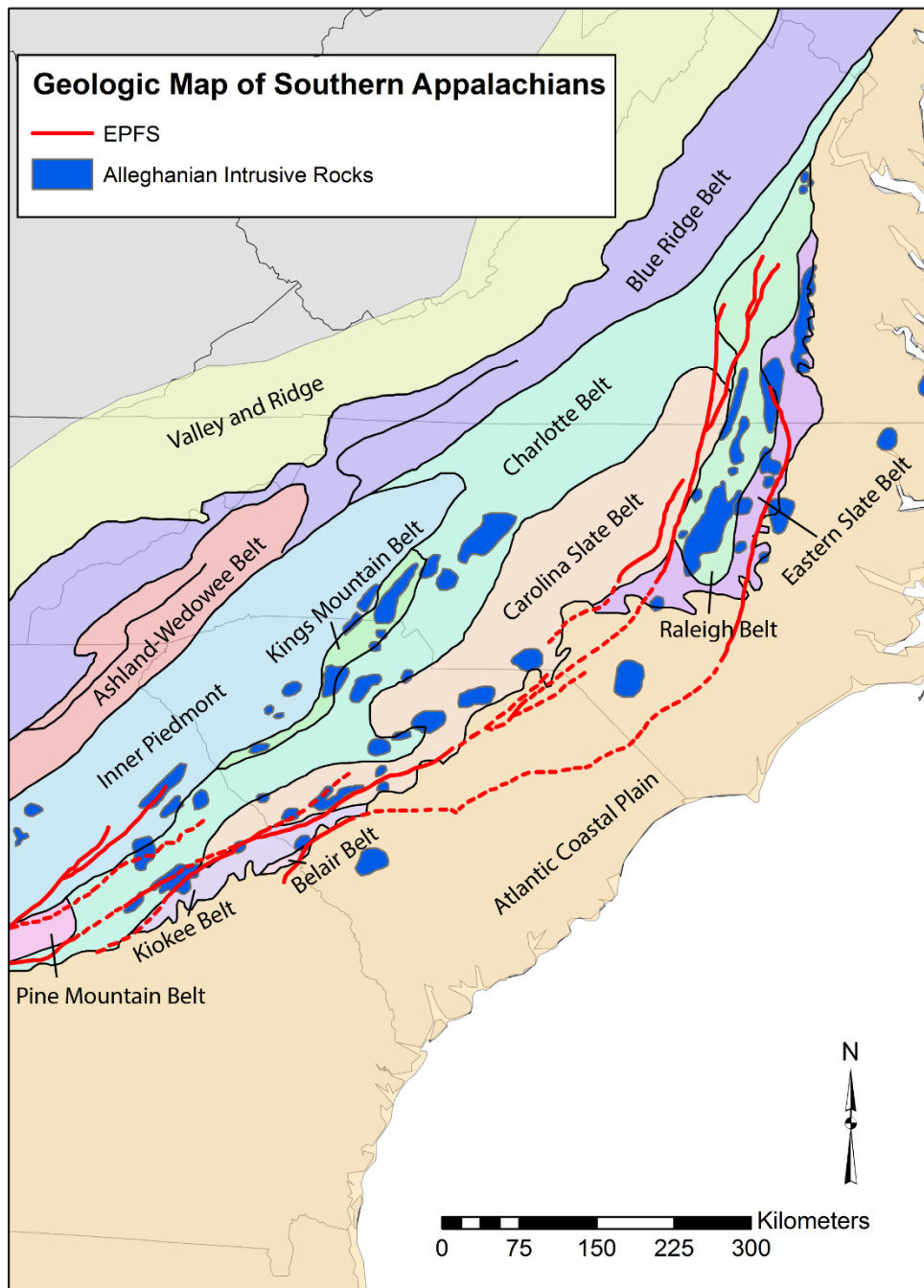
Figure 1. Simplified geologic map of the Southern Appalachians, including major geologic provinces, the Eastern Piedmont Fault system, and Alleghanian plutons. Modified from Hatcher et al. (1977); Bobyarchick (1981); Speer et al. (1994).

2. Geological Setting

2.1. Paleozoic Appalachian Tectonics

The Appalachian Mountains extend approximately 3000 km from the continental margin of Newfoundland, Canada, to the subsurface beneath the Coastal Plain in southern Alabama and Georgia (Hatcher, 2010). The mountain range is commonly subdivided into three regions: the northern Appalachians from Newfoundland to southern New York, the central Appalachians from southern New York to southern Virginia, and the southern Appalachians from southern Virginia to Alabama. While these three regions are part of the same large orogen, details of their geologic histories differ.

The Appalachians are an accretionary orogen that formed along the eastern margin of Laurentia following breakup of the supercontinent Rodinia. The Paleozoic history of the Appalachians involves three major deformational and metamorphic events: the Ordovician-Silurian Taconic, the Devonian-Mississippian Acadian, and the Pennsylvanian-Permian Alleghanian orogenies. The field area for this study in eastern North Carolina was strongly affected by the Alleghanian orogeny, which is therefore described in some detail here. The earlier two orogenies are considered only briefly.

The Taconic orogeny was the result of early collision between Laurentia and Gondwana, which produced widespread regional metamorphism and ductile deformation (Glover et al., 1983; Drake et al., 1989; Hatcher, 2010). In the northern Appalachians, a foreland fold-and-thrust belt formed from subduction produced amphibolite facies, as well as local granulite facies metamorphism. In the southern and central Appalachians, Taconic structures are poorly understood due to the strong overprint from later deformational events. However, Taconic

deformation was intense and polyphase into the interior of the orogen producing greenschist to amphibolite facies metamorphism.

The Acadian orogeny resulted from the zippered north-to-south closing of the Rheic ocean as Gondwanan superterranes collided with Laurentia (Hatcher, 2010). In the northern Appalachians, differential overthrusting and polyphase deformation produced high-grade metamorphism and abundant plutonism (Osberg et al., 1989). In the southern Appalachians, several ductile shear zones have been attributed to Acadian deformation and amphibolite facies metamorphism superimposed on rocks metamorphosed during the Taconic. In the central Appalachians, evidence of Acadian deformation and metamorphism is cryptic or absent. Therefore, it is unclear how Acadian metamorphism in the northern and southern Appalachians are related, although a connection may exist beneath the Coastal Plain in the central Appalachians.

The Alleghanian orogeny resulted from the late Paleozoic collision of Gondwana and Laurentia and is the major mountain-building event associated with the Appalachian chain (Hatcher et al., 1989; Hatcher, 2010). Collision began in the northeastern Appalachians and closed southward like a zipper as Gondwana rotated into head-on collision with southeastern Laurentia, ultimately resulting in the assembly of Pangea. Alleghanian deformation and metamorphism have been documented throughout the Appalachians and are commonly superimposed on rocks affected by earlier events. Based on seismic reflection data, much if not all of the northern and southern Appalachians are part of an enormous composite allochthonous sheet that lies above a deeply buried detachment surface (Ando et al., 1984).

In the northern Appalachians, Alleghanian deformation and metamorphism are restricted to the easternmost part of the orogen (Hatcher et al., 1989). Early Alleghanian deformation in the

northern Appalachians consists of brittle faults that form the margins of horsts and grabens. Most of these brittle faults were reactivated during ductile deformation exhibiting early sinistral motion followed by later dextral motion. Metamorphism in this region ranges from lower greenschist facies to sillimanite zone and typically decreases in intensity northward and eastward. Changes in metamorphic grade are abrupt and tend to be separated by faults.

In the southern and central Appalchians, a complex system of imbricated thrust sheets known as the Blue Ridge-Piedmont thrust sheet developed during the Alleghanian in the western part of the orogen. The eastern part of the orogen is dominated by plastic-to-brittle regional-scale zones of dextral transpression, known as the EPFS (Figure 1; Hatcher et al., 1977). Shear zones of the EPFS have moderately steep to subvertical mylonitic foliations and tend to separate rocks of contrasting metamorphic grade. Metamorphic intensities range from greenschist to amphibolite facies and appear to increase with proximity to major batholiths, suggesting metamorphism was roughly synchronous with plutonism. Brittle deformation does exist, but tends to be localized in zones of earlier ductile deformation.

Along with deformation and metamorphism, the Alleghanian orogeny is associated with a distinct 45 - m.y. - long magmatic event (Speer et al., 1994). Late Paleozoic plutonic rocks are widespread in the southern Appalachians (Figure 1) and consist mostly of granitoids, with only a small percentage of gabbroids. Calculated pressures of granitoid emplacement range from 2.1 to 5.1 kbar (~5-15 km in depth) and emplacement temperatures range from 710 to 790℃ (Vyhnal and McSween, 1990; Vyhnal et al., 1991). Many of these late Paleozoic plutonic rocks have a close spatial relationship with Alleghanian dextral shear zones. Between shear zones, where strain is low or absent, late Paleozoic plutonic rocks display weak fabrics and nearly circular shapes. Within or adjacent to shear zones, plutons are more abundant and have stronger fabrics

and more elongate and elliptical shapes. The deformed intrusions provide important evidence of the age, kinematics, location, and intensity of late Paleozoic deformation (Hatcher et al., 1989).

2.2. Regional Geology

The Piedmont of North Carolina is an important area in understanding the regional thermo-tectonic history of the southern Appalachians (Russell et al., 1985). The region includes several fault-bounded tectonostratigraphic terranes (Farrar, 1985a, Sacks, 1999). These terranes are comprised of tectonic blocks of an autochthonous or parautochthonous basement sequence of possible Grenville age overlain by other blocks of an allochthonous late Precambrian-early Paleozoic volcanogenic sequence.

The basement sequence consists of biotite-quartz-feldspar gneiss, biotite-hornblende-quartz-feldspar gneiss, pelitic gneiss, biotite-hornblende tonalitic to granodioritic gneiss, biotite-quartz-plagioclase gneiss, biotite granitic gneiss, and schist. These basement rocks are interpreted as being the southern extension of the Grenville-age Goochland terrane, based on petrographic correlation with dated rocks to the north in Virginia (Farrar, 1985a; Farrar, 1985b; Russell et al., 1985). The overlying volcanogenic sequence is composed of greenschist to amphibolite facies felsic and mafic volcanic rocks interlayered with volcanogenic sediments. Shallow intrusions appear to be part of the same sequence and range in composition from gabbro through tonalite to trondhjemite and quartz keratophyre. Although this sequence is undated, it is considered equivalent to the late Precambrian-early Paleozoic Carolina Slate Belt.

Both the basement and volcanogenic sequence have been intruded by numerous Paleozoic plutons. These plutons range in composition from hornblende-biotite tonalite to hornblende-biotite granite, biotite granite, and garnet-muscovite-biotite granite. The plutons of the eastern North Carolina Piedmont that have been dated range from 313 to 285 Ma (Russell et

7

al., 1985). Some of these plutons, or parts of them, have been deformed, while others are essentially undeformed.

In eastern North Carolina, the Piedmont includes several fault-bounded tectonostratigraphic terranes. From west to east these are the Carolina terrane, the Raleigh terrane, the Spring Hope terrane, the Triplet terrane, and the Roanoke Rapids terrane (Figure 2; Farrar, 1985a; Farrar, 1985b; Sacks, 1999). The Carolina terrane is bordered by the Nutbush Creek mylonite zone to the east (Sacks, 1999) and is composed of mainly metavolcanic and metasedimentary rocks (Secor et al., 1983). The Raleigh terrane is bound in the west by the Nutbush Creek mylonite zone, Lake Gordon mylonite zone, and Hylas fault zone, while the Macon fault zone is the eastern boundary (Russell et al., 1985; Stoddard et al., 1991; Sacks, 1999). The Raleigh terrane is composed of amphibolite facies schists and gneisses locally overprinted by greenschist facies metamorphism. These schists and gneisses were metamorphosed and intruded by numerous late Paleozoic granitic plutons. The Spring Hope terrane is separated from the Raleigh terrane by the Macon fault zone, while the eastern boundary is the Hollister mylonite zone. The Spring Hope terrane consists of metasedimentary rock, felsic and mafic metavolcanic rocks of greenschist facies and epidote-amphibolite facies schist, gneiss and phyllite. The Triplet terrane is a narrow, elongate block of gneiss and schist juxtaposed between the Hollister mylonite zone to the west and the Gaston Dam fault to the east. Rocks in the Triplet terrane consist predominantly of medium- to coarse-grained biotite gneiss with some biotite-muscovite schist, and granitic gneiss. The Roanoke Rapids terrane includes the metavolcanic and metasedimentary rocks east of the Gaston Dam fault and the Hollister mylonite zone. Rocks in this area have been metamorphosed to greenschist-amphibolite facies, similar to those of the Spring Hope terrane, and consist of slaty to phyllitic metasedimentary rocks as well

8

as metavolcanic and hypabyssal rock of the mafic-ultramafic Halifax County Complex (Sacks, 1999).
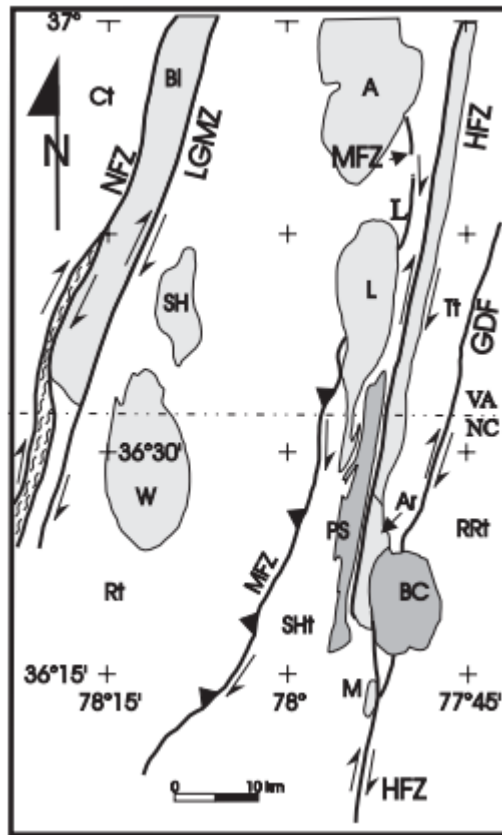
Figure 2. Geologic map of tectonostratigraphic terranes in the eastern Piedmont of North Carolina and Virginia. From Sacks (1999). Ct = Carolina terrane, Rt = Raleigh terrane, SHt = Spring Hope terrane, Tt = Triplet terrane, RRt = Roanoke Rapids terrane.

Metamorphic and deformation events of the eastern North Carolina Piedmont have been described in detail by Farrar (1985b). Three major metamorphic events affected the region (Farrar, 1985b; Russell et al., 1985). The basement sequence was metamorphosed to the sillimanite zone during the early (Grenville ?) M_g event. The M_1 (Taconic ?) event metamorphosed the volcanogenic sequence to greenschist facies. It is unclear if this event affected the basement sequence because it was later overprinted by a higher grade metamorphic event. The M_2 event metamorphosed the already juxtaposed sillimanite zone assemblages of the basement sequence and the chlorite zone volcanogenic sequence to upper greenschist and

9

amphibolite facies. This event was accompanied by the intrusion of numerous late Paleozoic granites, including the Butterwood Creek pluton. The timing of the thermal maximum is not known, however cooling from this maximum took place between ~260 and 245 Ma making it at least partially an Alleghanian event (Russell et al, 1985).

Along with the three major metamorphic events, four major deformation events have been defined in the eastern Piedmont of North Carolina (Farrar, 1985b; Russell et al., 1985). The D_g event, possibly a combination of several component events, occurred under M_g conditions and produced compositional layering, penetrative foliation, and isoclinal folds in rocks of the basement sequence. Since this event only occurred within the basement sequence it is interpreted as being a Grenville deformation event. The D_1 event produced penetrative foliation and minor isoclinal folding of pre-existing compositional layering within the volcanogenic sequence under M_1 conditions. The D_2 event thrust the volcanogenic sequence over the basement sequence, resulting in the juxtaposition of the two sequences along a regional decollement. D_2 deformation appears to be Taconic, however the Castalia granite (313 ± 13 Ma) and Butterwood Creek granite (292 ± 31 Ma) both cut the decollement suggesting the D_2 event could be as young as Acadian but must be pre-Alleghanian. D_3 deformation produced regional folds and mylonite zones. The Nutbush Creek, Macon, and Hollister mylonite zones formed during this event along the limbs of regional folds (Figure 3). The Hollister mylonite zone cuts the Butterwood Creek pluton, which lies in both the Raleigh belt and the Eastern slate belt. The parts of the pluton in the Raleigh belt are foliated, where the parts in the Eastern slate belt are essentially undeformed. Thus, D_3 deformation is at least part Alleghanian, occurring during the intrusion of Alleghanian plutons and before regional cooling.
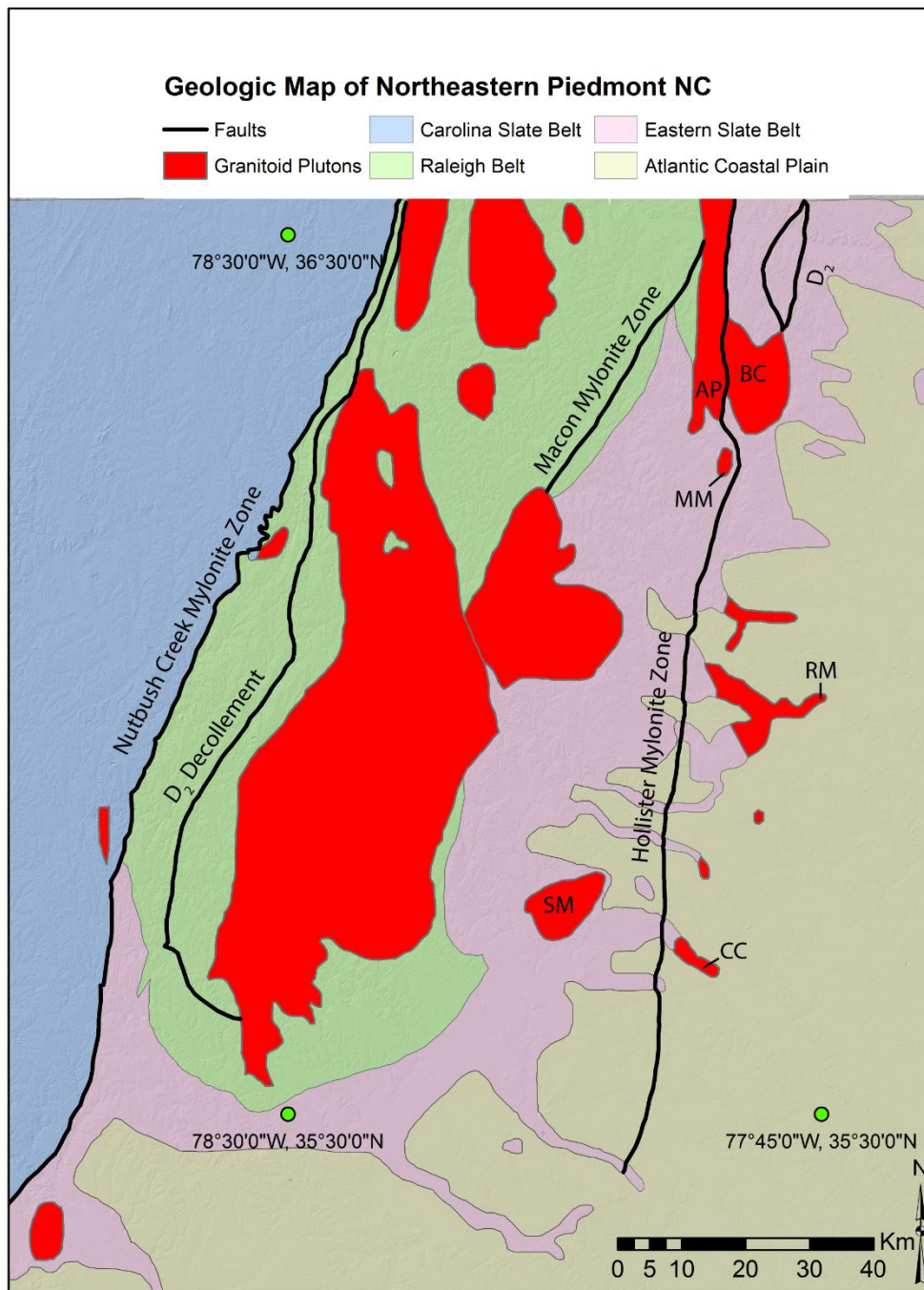
Figure 3. Geologic map of major belts, fault zones, and Alleghanian plutons in the northeastern Piedmont of North Carolina. Rb-Sr whole-rock ages of granite plutons in the Eastern Slate Belt include: AP: Airlee Pluton, 251 Ma (Russell et al., 1985); BC: Butterwood Creek pluton, 292 $\pm$ 31 Ma (Russell et al., 1985); MM: Medoc Mountain, 301 $\pm$ 6 Ma (Fullagar and Butler, 1979); RM: Rocky Mount, 345 $\pm$ 1 Ma (Moncla, 1990); SM: Sims, 287 $\pm$ 9 Ma (Wedemeyer and Spruill, 1980). U-Pb zircon ages of granite plutons include: CC: Contentnea Creek, 305.7 $\pm$ 0.22 Ma (this study). Modified from Russell et al. (1985).

2.3. Study Area

The study area is located in southern Wilson County, North Carolina, along the eastern edge of the Eastern Slate Belt (Figure 4). The HMZ, part of the EPFS, runs through the western part of Wilson County. In this region, outcrops of Paleozoic rocks are scarce as most basement rock is covered by Cenozoic sediments of the Coastal Plain.

2.3.1. *Hollister mylonite zone*

The EPFS is a major late Paleozoic transpressional tectonic boundary that stretches from Alabama to Virginia (Figure 1; Hatcher et al., 1977; Bobyarchick, 1981). The HMZ is the easternmost component of the EPFS and is a major lithotectonic boundary. In some locations the HMZ separates the Raleigh Belt to the west from the Eastern Slate Belt to the east, although for most of its length, it passes through the Eastern Slate Belt (Figure 3; Farrar, 1985b). The HMZ is a steeply westward dipping, generally north-south striking mylonite zone that extends from southeastern Virginia into northeastern North Carolina (Fletcher, 1992). Aeromagnetic data suggest the HMZ merges to the south with the Augusta fault (Hatcher et al., 1977) under Coastal Plain cover in South Carolina and Georgia. The Paleozoic slip history of the HMZ is dominated by dextral strike-slip motion with a minor dip-slip component. Hornblende-in-aluminum geobarometry in the Butterwood Creek pluton suggest maximum displacement of 15.1 ± 2.7 km and a minimum vertical displacement of 3.9 ± 2.7 km during and since the Alleghanian (Vyhnal and McSween, 1990). Brittle reactivation of the HMZ in the Alleghanian has been hypothesized in response to post-metamorphic differential uplift (Russell et al., 1985; Stoddard et al., 1991), although no conclusive evidence has been published.

2.3.2. Alleghanian magmatism associated with the HMZ

The HMZ cuts crystalline rocks of the eastern Piedmont in North Carolina and Virginia (Sacks, 1999). Granite was intruded as sheets into the metavolcanic rock and deformed along Reidel shears associated with the HMZ. Plutons that intruded the Raleigh Belt tend to be foliated, whereas those that intruded the Eastern Slate Belt tend to be unfoliated (Russell et al., 1985). The foliated portions of plutons indicate dextral shear for the fault zone, and local brittle fabrics suggest additional younger movement (Russell et al., 1985; Sacks, 1999). Syntectonic plutons are instrumental in understanding the timing and kinematics of the HMZ.

2.3.3. Contentnea Creek pluton

The Contentnea Creek granite is a previously unstudied intrusion that lies within the Eastern Slate Belt, in southern Wilson County, North Carolina (Figure 4). The pluton is mostly covered by Coastal Plain sedimentary strata, but available exposure suggests the pluton is an approximately 20 km^2 northwest-southeast elongate body (Figure 5). Gravity data suggest the western margin of the pluton may be truncated or deformed by the nearby HMZ (Lawrence, 1999). Recent investigation (Burns and Horsman, 2013) shows the pluton has clear variations in fabric intensity and orientation. The eastern margin of the pluton, away from the mylonite zone, displays magmatic fabrics. In contrast, the western margin of the pluton, near the HMZ, has a high-temperature solid-state fabric consistent with syntectonic emplacement in an active shear zone. Locally, the high-temperature solid-state fabric is overprinted by both a low-temperature solid-state fabric and distinct shear fractures. The major goal of this thesis is to study the Contentnea Creek granite with a wide range of tools to better understand how it fits in with the late Paleozoic regional geology.
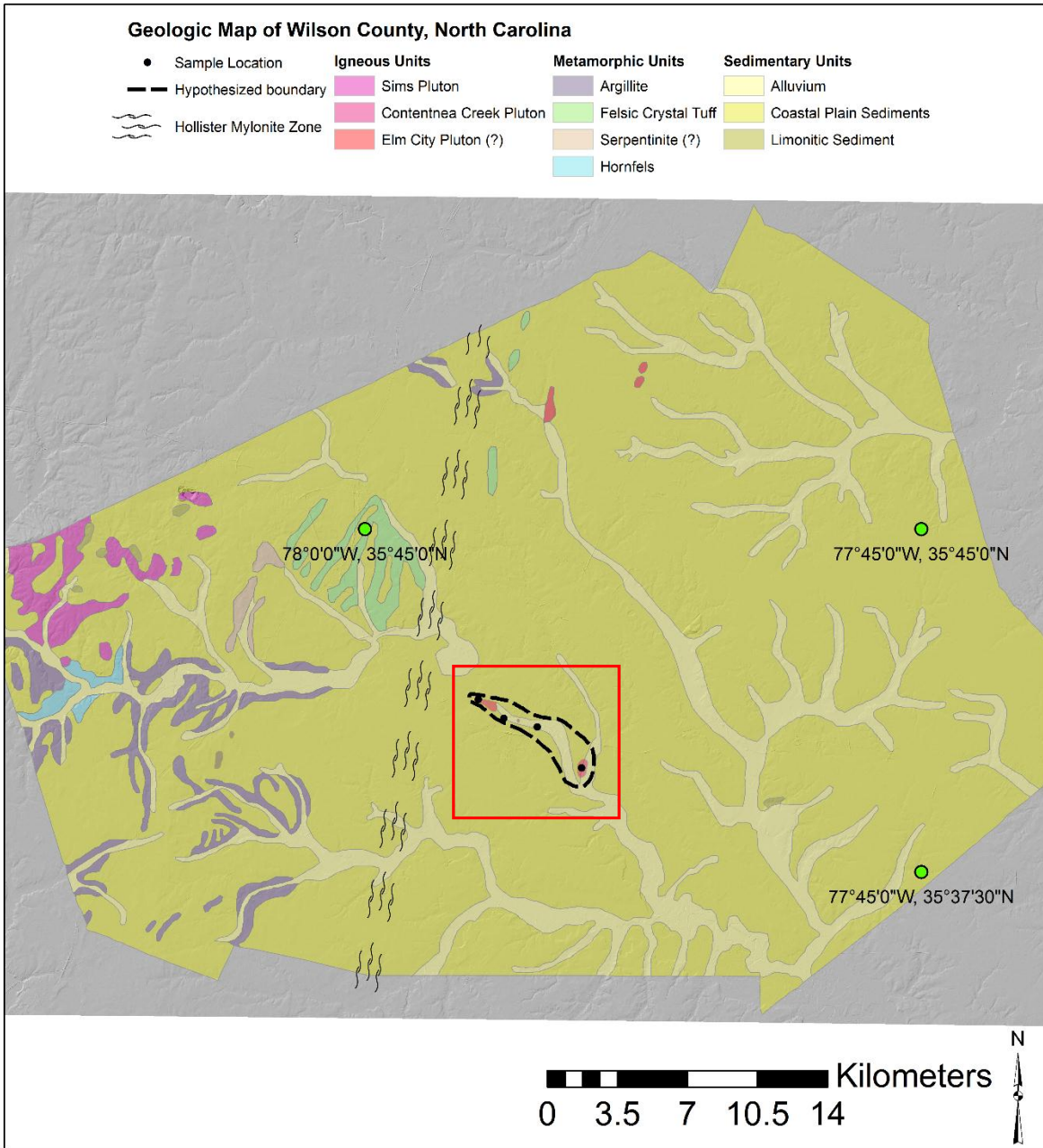
Figure 4. Geologic map of Wilson County, North Carolina with the study area outlined in red. Modified from Wilson (1979).
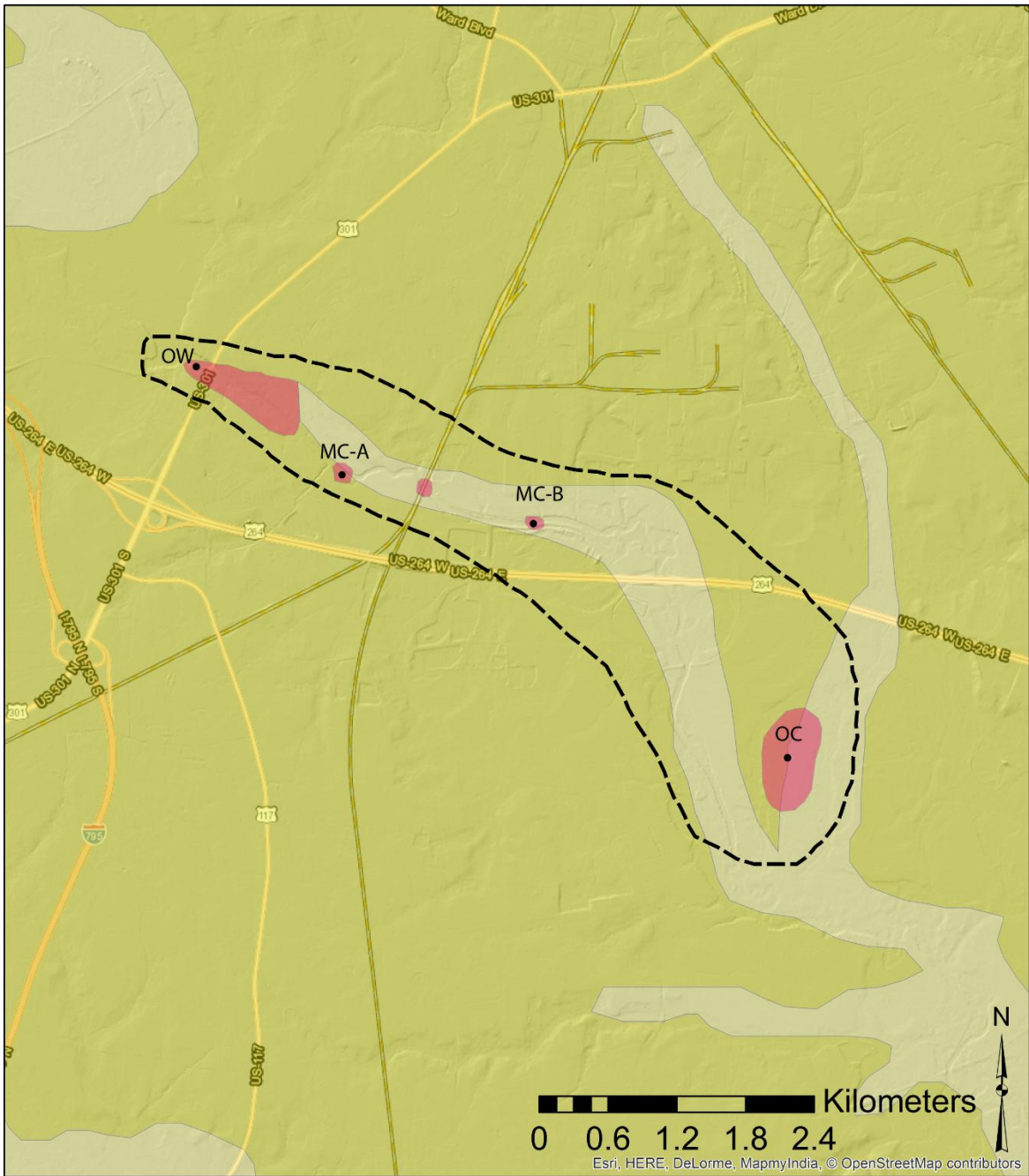
Figure 5. Geologic map of the study area around the Contentnea Creek pluton with sample locations labeled and dashed lines indicating inferred area underlain by the Contentnea Creek pluton. Modified from Wilson (1979).

3. Methods and Results

The Contentnea Creek pluton is exposed over a series of small, isolated outcrops. Hand samples were collected where possible, and shallow drill cores were collected from some outcrops. Good exposure exists at Wiggins Mill on Wiggins Mill Road and in the Martin Marietta rock quarry on Black Creek Road. Exposures also exist locally along Contentnea Creek and are most easily accessed by canoe.

3.1. Petrography

Polished thin sections from twelve samples were analyzed petrographically. Due to poor exposure and extensive weathering of outcrops, thin section petrography provides an opportunity to observe textures and structures that cannot be recognized at outcrop and hand-sample scales.

3.1.1. Observations

The Contentnea Creek pluton is a coarse-grained biotite granite; major minerals are quartz, alkali feldspar, plagioclase, and biotite. Alkali feldspars are abundant (~35%) and include euhedral to subhedral megacrysts up to ~3 cm. Plagioclase is less abundant (~30%) and range from ~2 to 14 mm. Quartz (~25%) ranges from ~ 3 to 10 mm. Biotite is least abundant (~10%) ranging from ~1 to 5 mm. Trace minerals include apatite, zircon, muscovite, magnetite, and titanite. Mineralized shear fractures are dominated by epidote. Alteration of feldspars to phyllosilicates is common, and alteration products include muscovite, sericite, and kaolinite. Alteration of biotite to chlorite is also common, especially on the western margin of the pluton. No major mineralogical variations exist between available exposures. However, textural and deformation variations are observed at different locations.

The eastern margin of the Contentnea Creek pluton displays more magmatic textures (Figure 6A). Feldspars and biotite are less deformed compared to the western margin (Figure 6B,

C). Some bending in feldspars and quartz recrystallization is present but there is no evidence of microbrecciation.
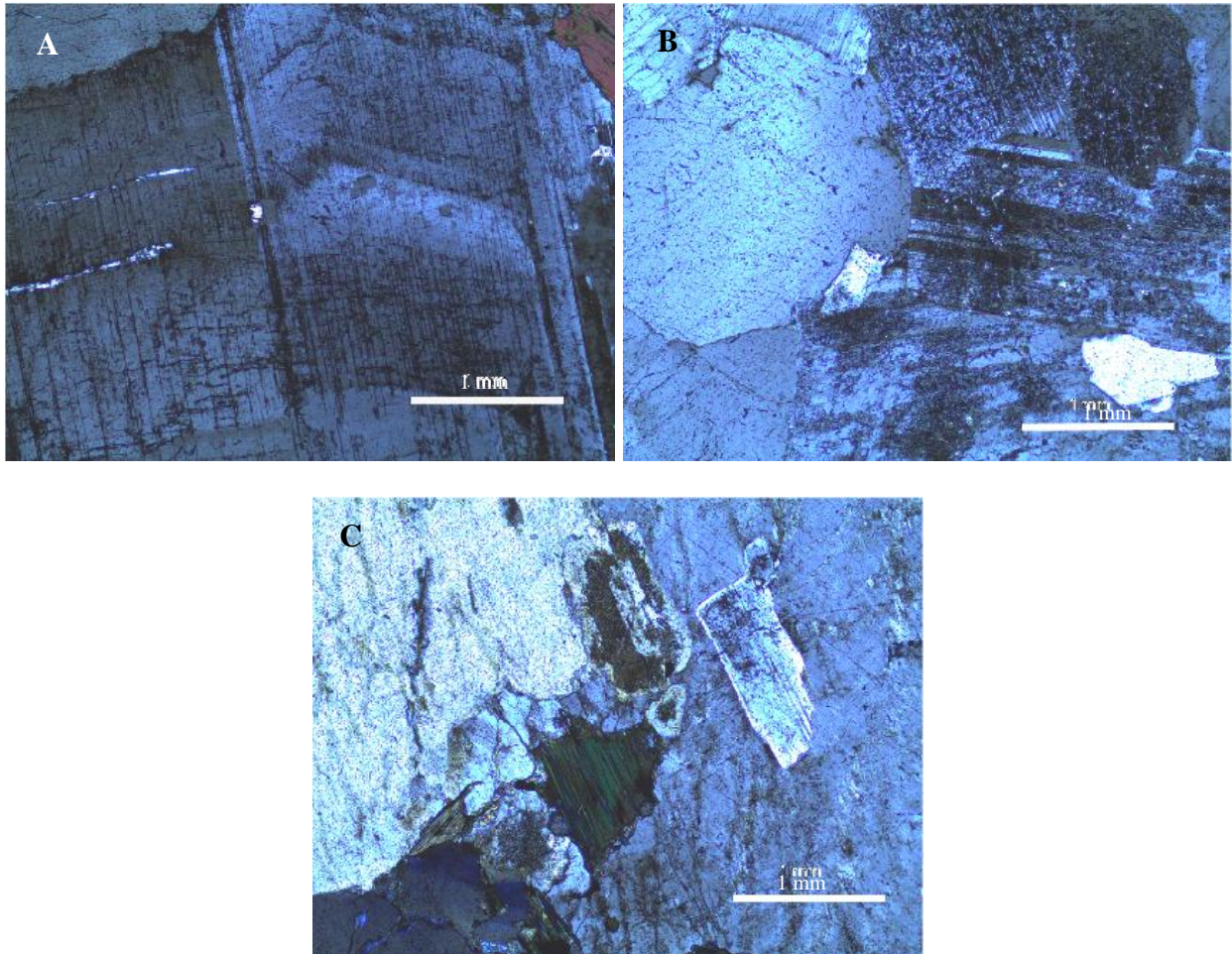
Figure 6. Photomicrographs of the eastern margin of the Contentena Creek pluton in cross-polarized light. (A) Undeformed feldspar crystal. (B) Less deformed feldspar crystal compared to the western margin. (C) Less deformed biotite compared to the western margin.

The western margin of the Contentnea Creek pluton displays three distinct fabrics: a high-temperature solid-state (HTSS) fabric, a cross-cutting low-temperature solid-state (LTSS) fabric, and mineralized shear fractures (Figure 7). The HTSS deformation is recognized by bent twinning in feldspars and bent biotite, and evidence of recrystallized quartz (Figure 7A). The

LTSS deformation is recognized by microbreccias (Figure 7B). Shear fractures are recognized by mineralized planar features that cross-cut HTSS deformation (Figure 7C).
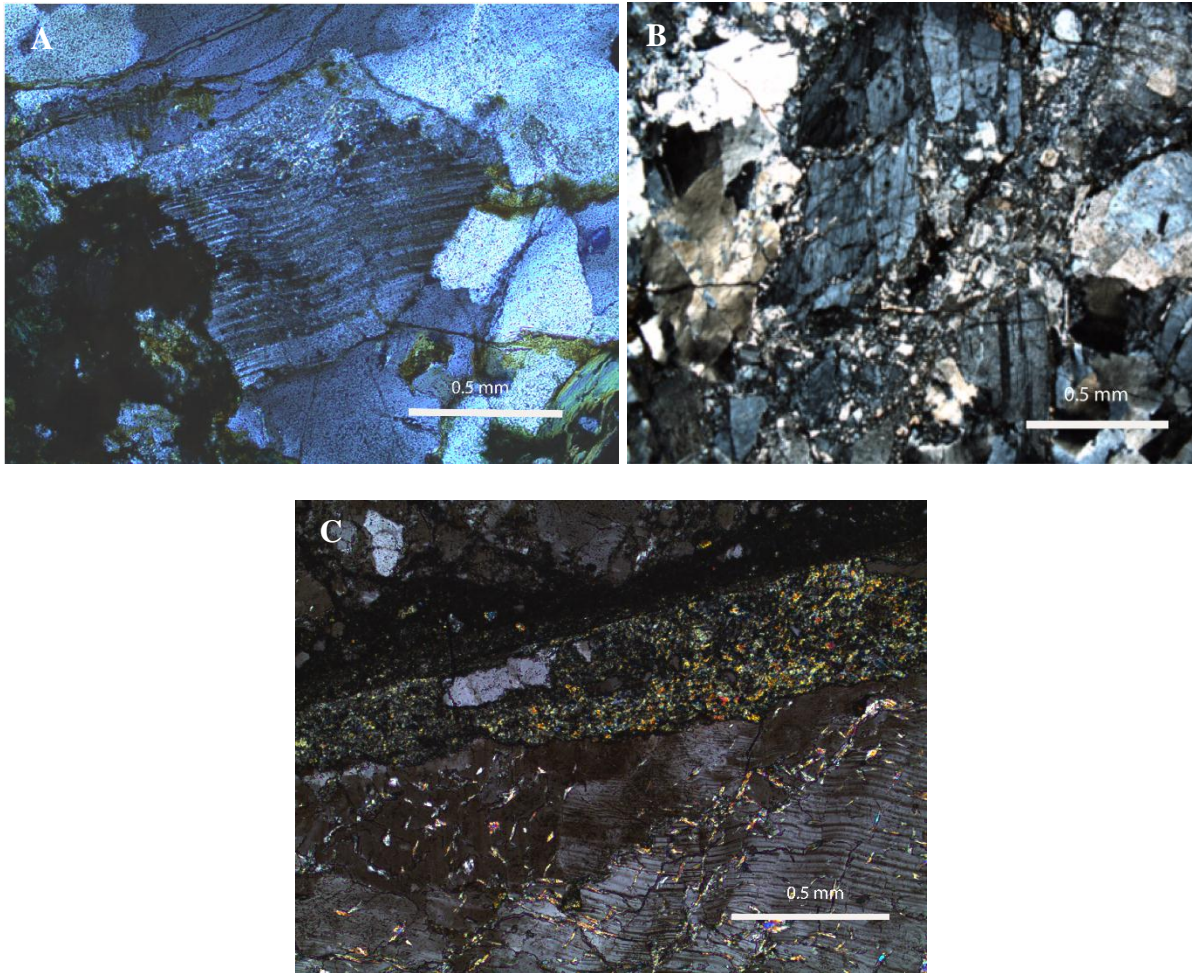
Figure 7. Photomicrographs from the western margin of the Contentnea Creek pluton in cross-polarized light. (A) HTSS fabric in deformed feldspar. (B) LTSS fabric in microbreccias. (C) Shear fracture cross-cutting HTSS fabric.

The central parts of the pluton also display evidence of HTSS fabrics in bent micas (Figure 8A). Possible LTSS fabrics exists in recrystallization of quartz crystals (Figure 8B). Alteration of feldspars to phyllosilicates, possibly muscovite, kaolinite, and sericite, is common (Figure 8C). The central parts of the pluton consist of smaller and more recrystallized quartz crystals compared to the pluton margins.
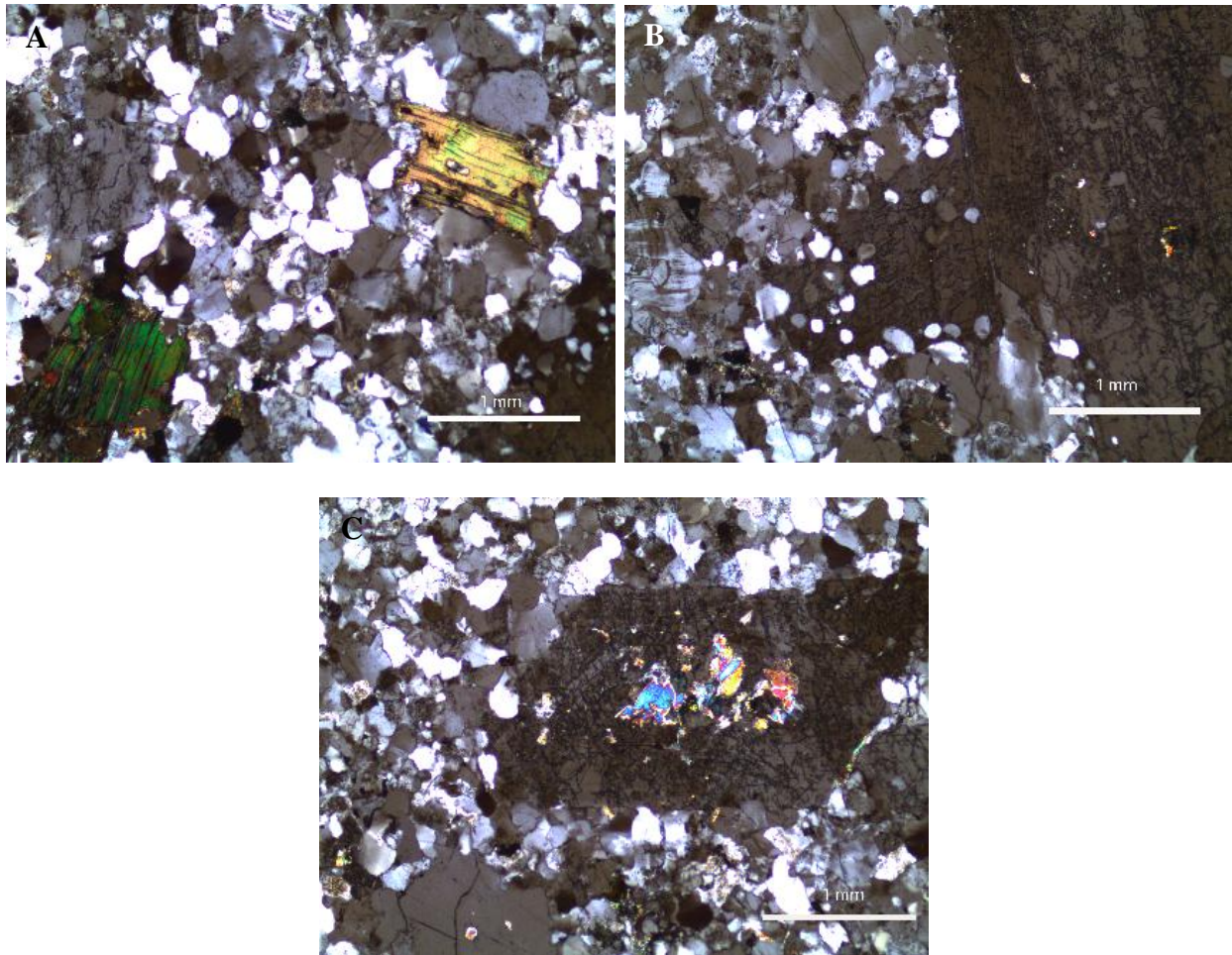
Figure 8. Photomicrographs from the central parts of the Contentnea Creek pluton in cross-polarized light. (A) HTSS fabric in bent mica. (B) Possible LTSS fabric in quartz recrystallization. (C) Alteration of feldspars to phyllosilicates.

3.2. Shape Preferred Orientation Fabric Analysis

Shape preferred orientation (SPO) analysis in rocks provides a quantitative measure of rock fabric (Launeau et al., 1990; Launeau and Cruden, 1998). In igneous rocks, fabrics are usually defined by mean elongation directions of crystals. SPO analyzes the shape and orientation of crystal populations on a 2-D plane and fits them on an ellipse.

Two samples from the Contentnea Creek pluton were analyzed using SPO; one from the western margin closer to the mapped fault zone and one from the eastern margin away from the mapped fault zone. Each sample was cut with a rock saw to have three mutually perpendicular

planar surfaces (Figure 9A). Each face was then scanned and manipulated by taking away the

weathered borders and creating a two-color binary image by isolating dark minerals (biotite and

oxides) with the threshold tool (Figure 9B). Each image was analyzed with the SPO2003

computer program (Launeau and Robin, 2005). A two-dimensional shape fabric ellipse of the

dark grains was calculated for each image by the intercept method. The intercept method is based

on counting the number of intercepted segments of an object by a set of parallel lines in a

number of directions (Launeau et al., 2010). Three-dimensional ellipsoids were calculated

mathematically by combining 2-D data from all three faces in the program Ellipsoid2003. Using

the principal axes of the SPO ellipsoid several scalar parameters can be calculated. The mean

shape factor (T) quantifies the shape of the ellipsoid with respect to a sphere. A purely prolate

ellipsoid would have a T value of -1 and a purely oblate ellipsoid would have a T value of 1,

where a sphere has a T value of 0. The degree of anisotropy (P_j) quantifies fabric intensity, where

higher values have stronger fabrics.

$$T = [2\ln(K_2/K_3)/\ln(K_1/K_3)]-1, \text{ and}$$
$$P_j = \exp(2[(\eta_1-\eta_b)^2 + (\eta_2-\eta_b)^2 + (\eta_3-\eta_b)^2]^{1/2}).$$
Where K_1 is the long axis,

K_2 is the intermediate axis,

K_3 is the short axis of the ellipsoid, and

$\eta_i = \ln K_i$ and $\eta_b = \ln(\eta_1 \times \eta_2 \times \eta_3)^{1/3}$.

OW-2   OC-2

6 cm
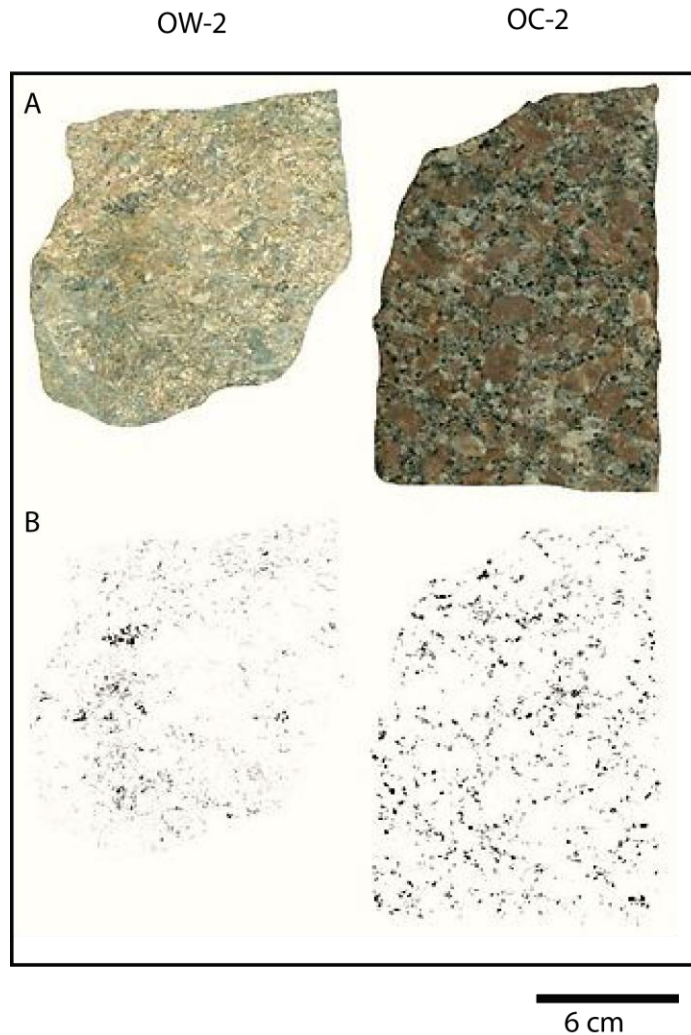
Figure 9. (A) Scanned images of one cut sample face for SPO analysis for two samples. (B) Threshold images show dark grains (biotite and oxides) to be analyzed by the intercept method.

Fabric orientation results for SPO analysis are plotted on equal angle, lower hemisphere stereographic projections in Figure 10. The foliation on the western margin of the Contentnea Creek pluton from sample OW-2, close to the nearby fault zone, strikes N-S and dips moderate-steeply to the east, with a shallowly south-plunging lineation. The mean calculated degree of anisotropy from the western margin is 1.095 and the mean shape factor is neutral, with a value of 0.014. The foliation on the eastern margin of the Contentnea Creek pluton from sample OC-2, away from the fault zone, strikes NW-SE and dips steeply to the northeast, with a steeply

southeast-plunging lineation. The mean calculated degree of anisotropy from the eastern margin is 1.105 and the mean shape factor is predominantly prolate, with a value of -0.612.
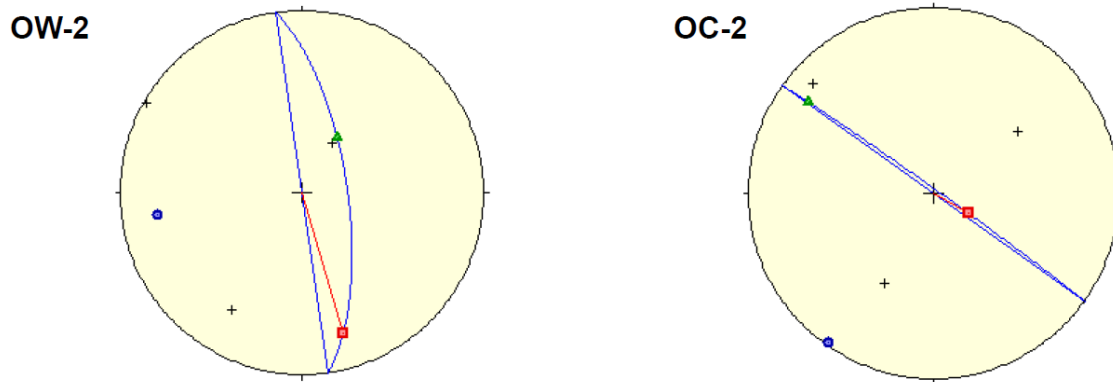
Figure 10. Lower hemisphere stereographic projections showing 3-D orientations of SPO fabric in the Contentnea Creek pluton. OW-2 represents the western margin of the pluton. The strike and dip of the foliation plane is 352/70, the plunge and trend of the lineation is 21-> 163. OC-2 represents the eastern margin of the pluton. The strike and dip of the foliation plane is 306/88, the plunge and trend of the lineation is 72->120. The blue arcs represents the foliation plane defined by the SPO of the black minerals. The red line represents the lineation on the foliation plane. The red square is the long axis, the green triangle the intermediate axis, and the blue circle the short axis of the fabric ellipsoid. Small black plus signs show poles to the plane of the three analyzed axes for each sample.

3.3. Anisotropy of Magnetic Susceptibility Fabric Analysis

Anisotropy of magnetic susceptibility (AMS) is a technique for measuring magnetic fabrics of oriented samples (Rochette et al., 1992). AMS is especially useful for analyzing weak fabrics like those commonly developed in igneous rocks and where poor exposure and field measurements may be difficult to obtain (Rochette et al., 1992; Bouchez, 1997; Tomezzoli et al., 2003; Horsman et al., 2005). A material placed in a magnetic field becomes magnetized. The relationship between the inducing and resulting fields is described by the susceptibility. The results of AMS measurements include a fabric ellipsoid which defines the length and orientation of the long (K_1), intermediate (K_2), and short (K_3) principal axes. The shapes and orientations of fabric ellipsoids in igneous rocks can be related to magmatic flow, however, in deformed igneous rocks, deformation may control their orientations. Iron is the principal element responsible for the magnetic signal (Bouchez, 1997).

22

It is important to characterize the magnetic mineralogy for proper interpretations of magnetic fabrics. Iron-bearing minerals produce different susceptibility magnitudes as a function of iron content for different morphologies. Paramagnetism is the slightly positive magnetic susceptibility generated by Fe-bearing silicates, which, in granitoids, includes phyllosilicates, amphiboles, ilmenite, pyroxene, cordierite, garnet, and tourmaline. Ferromagnetism has a strongly positive susceptibility at low field strength. Magnetite along with accessory monoclinic pyrite are the main ferromagnetic minerals in granites. Anitferromagnetic minerals, hematite and goethite, produce susceptibility values lower than paramagnetic minerals. Diamagnetic susceptibility is slightly negative and is affected by every mineral.

Like in SPO analysis using the magnitudes of the principal axes (K_1, K_2, K_3) several scalar parameters can be calculated. In addition to the mean shape factor (T) and the degree of anisotropy (P_j), bulk susceptibility (K_m), a measure of abundance and variety of magnetic grains, can be calculated.

$$K_m = (K_1 + K_2 + K_3)/3.$$

Ten oriented 25-mm-diameter cores from two sites were collected in the field from the central parts of the pluton using a portable rock drill and four 25-mm-diameter cores from two sites were collected from oriented hand samples using a drill press from margins of the pluton. From these cores 22-mm-long cylindrical specimens were cut. Low-field AMS was measured on each specimen using the AGICO MFK1-A Kappabridge at East Carolina University operating at a frequency of 976 Hz with a field intensity of 200 A/m peak. Software supplied with the instrument was used to compile data.

A total of 30 specimens from 5 sites were analyzed using AMS (Appendix A). Fabric results from site OW display small error ellipses with mean K_1 orientations that plunge moderately to shallowly to the southwest and mean K_3 orientations plunge shallowly to the

north-northwest on the western margin of the Contentnea Creek pluton (Figure 11A). Results from site MC-A, from the central portion of the pluton, also display small error ellipses, with mean K_1 orientations that plunge moderately to shallowly to the southwest and mean K_3 orientations plunge moderately to steeply to the northeast (Figure 11B). Results from site MC-2, taken just a few meters away from MC-A, did not contain enough data for statistical analysis however, results are internally consistent with K_1 orientations that plunge shallowly to the southeast-northwest and K_3 orientations that plunge steeply to the northeast (Figure 11C). Results from site MC-B, also from the central portion of the pluton, display large error ellipses with mean K_1 orientations from steeply to moderately plunging to the northwest and mean K_3 orientations that plunge shallowly to the northeast (Figure 11D). Results from site OC display small error ellipses with mean K_1 orientations that plunge shallowly to the southwest and mean K_3 orientations that plunge moderately to steeply to the southeast on the eastern margin of the pluton (Figure 11E).
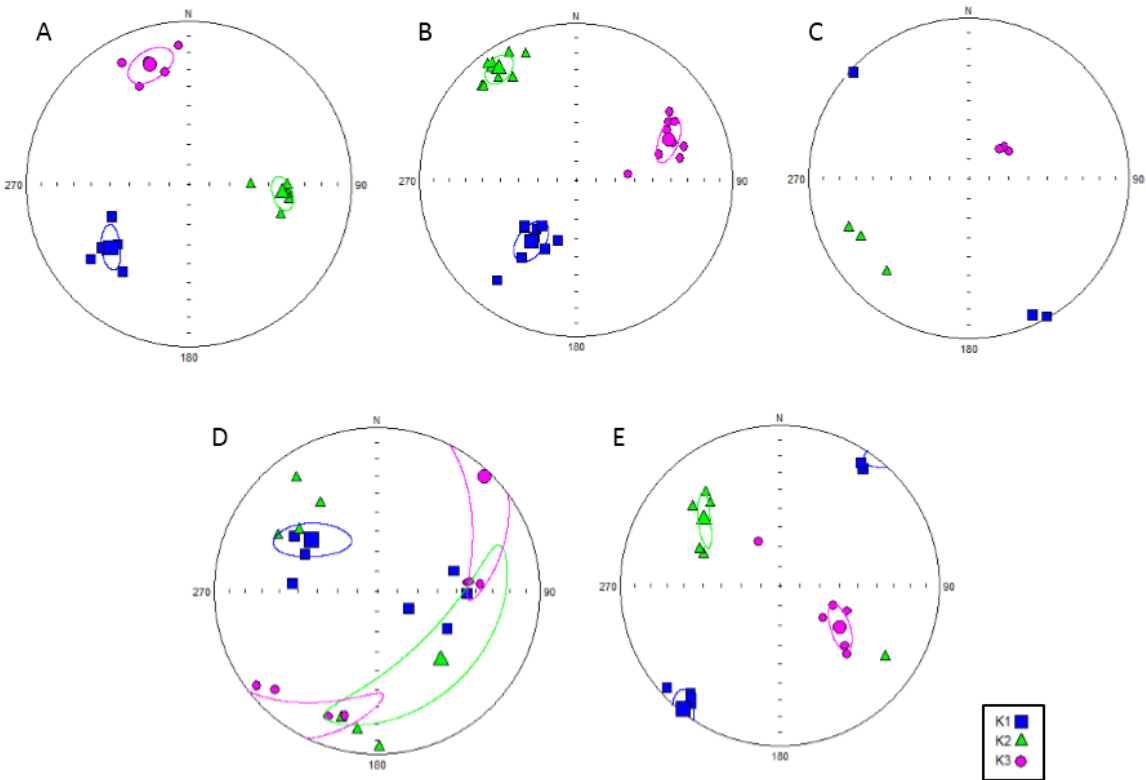
Figure 11. Lower hemisphere stereographic projections of measured AMS axes from the Contentnea Creek pluton. (A) OW, from the western margin. (B) MC-A, from the internal parts of the pluton. (C) MC-2, from the internal parts of the pluton. (D) MC-B, from the internal parts of the pluton. (E) OC, from the eastern margin of the pluton.

Bulk susceptibility (K_m) values range from 753-30921 µSI (Figure 12A, C). Samples from the western margin of the pluton, closest to the HMZ, tend to have the lowest K_m values (1974 µSI average), while those from the eastern margin of the pluton, farthest away from the HMZ, tend to have the highest K_m values (26485 µSI average). The central parts of the pluton show more variable K_m values. MC-A has a K_m average of 20810 µSI while MC-2 has a K_m average of 12635 µSI (calculated). MC-B has a K_m average of 10140 µSI.

Values of the degree of anisotropy (P_j) range from 1.102 to 1.322 (Figure 12B, C). The margins of the pluton have similar P_j values, with the western margin samples P_j averaging 1.138 and the eastern margin samples average 1.136. MC-A from the central part of the pluton has the highest P_j average at 1.186, while MC-B is more similar to the margins averaging 1.131.

Values for the shape parameter (*T*) range from -0.896 to 0.885 (Figure12A, B). The western margin of the pluton averages a dominantly oblate shape fabric of 0.328. MC-A from the central part of the pluton averages a neutral shape fabric of 0.009, while MC-B, also from the central part of the pluton averages a dominantly oblate shape fabric of 0.314. The eastern margin of the pluton averages a fairly dominate prolate fabric shape of -0.183.
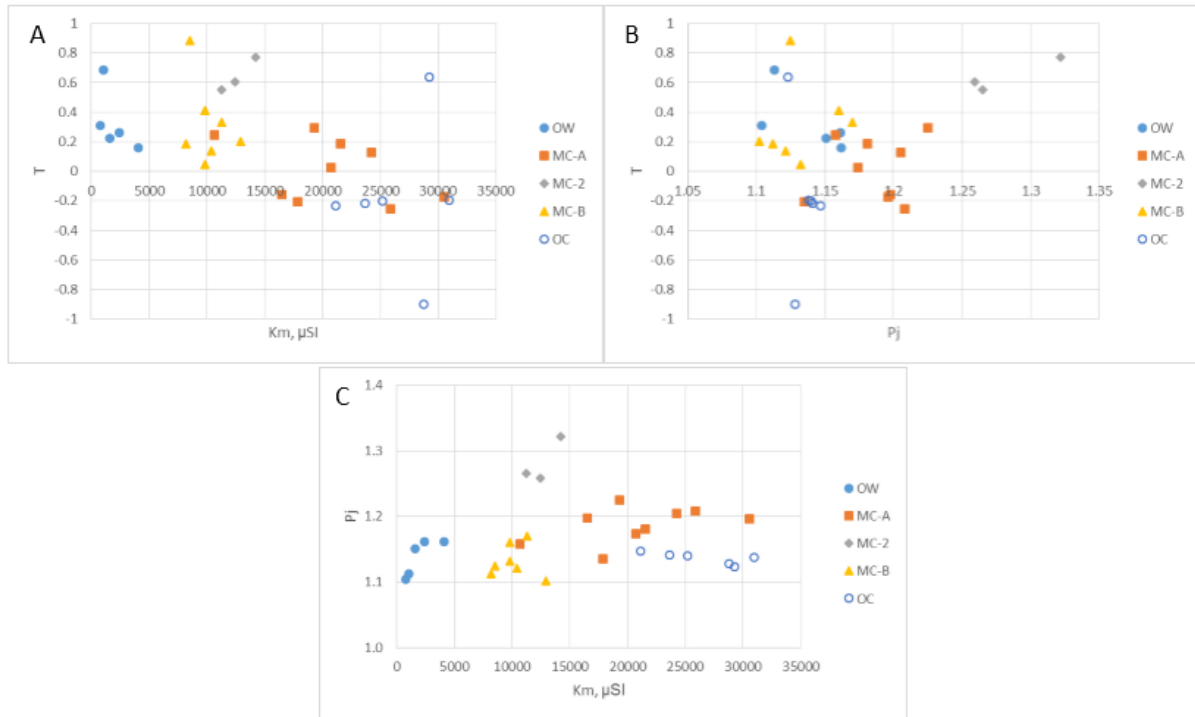
Figure 12. Plots of AMS scalar parameters. (A) Shape parameter vs. bulk susceptibility. (B) Shape parameter vs. degree of anisotropy. (C) Degree of anisotropy vs. bulk susceptibility.

3.4. Geochemistry

Whole rock major and trace element geochemical data from four sites were analyzed using inductively coupled plasma mass spectrometry (ICP-MS; Montaser, 1998) by Acme Analytical Laboratories, Vancouver, B.C., Canada. Major and trace element geochemistry data were used to make comparisons with other Alleghanian age intrusions.

Silica contents of the Contentnea Creek pluton range from 71.64 – 75.48 wt%, which is close to the mean silica content of Alleghanian plutons (71.40 wt%; Speer and Hoff, 1997). The pluton is subalkaline on the basis of total alkali ($Na_2O + K_2O$ wt%) versus silica, with K_2O greater than Na_2O, which is also consistent with other Alleghanian plutons (Figure 13). A nearly linear negative trend with increasing SiO_2 is well-defined for all major elements (Al_2O_3, CaO, P_2O_5, TiO_2, MgO, Fe_2O_3) in Alleghanian plutons as well as for the Contentnea Creek pluton (Figure 14).
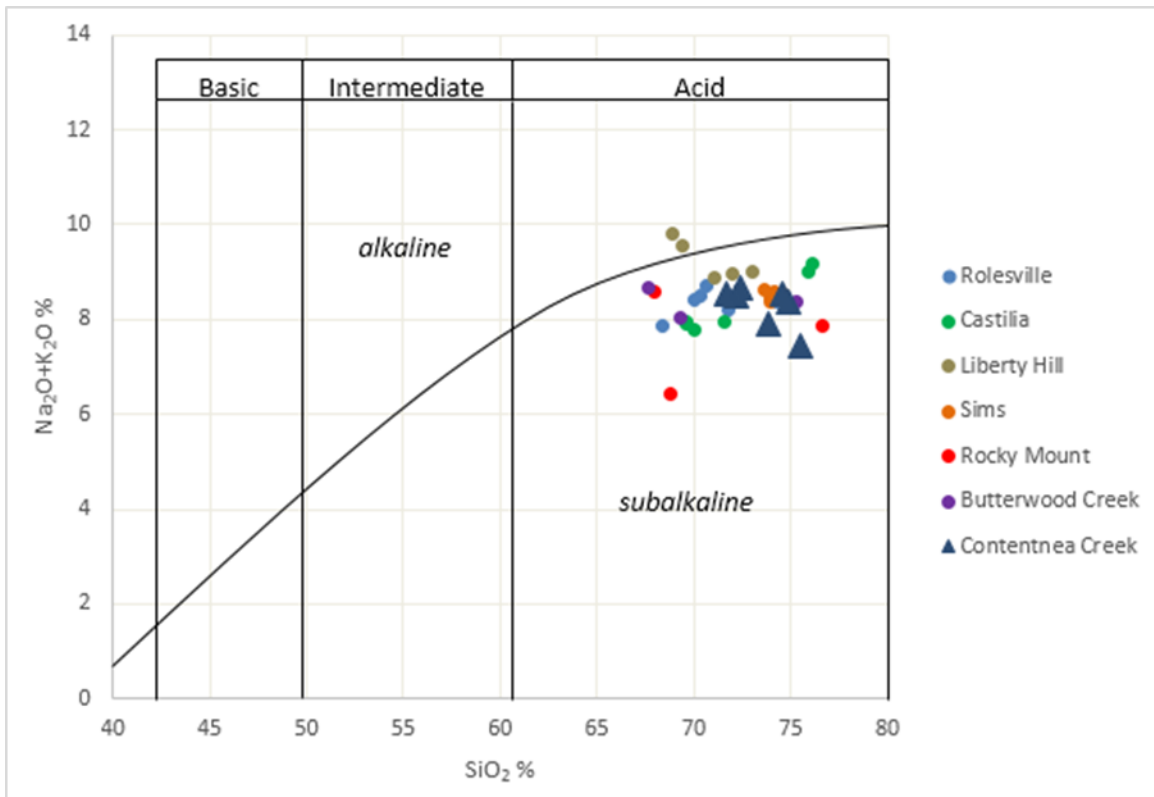
Figure 13. Total alkalis ($Na_2O + K_2O$ wt. %) versus silica (SiO_2 wt. %) diagram. Data for Rolesville, Castilia, Liberty Hill, and Sims plutons from Speer and Hoff (1997). Data for Rocky Mount and Butterwood Creek plutons from Coler et al. (1997). Contentnea Creek data from this study.
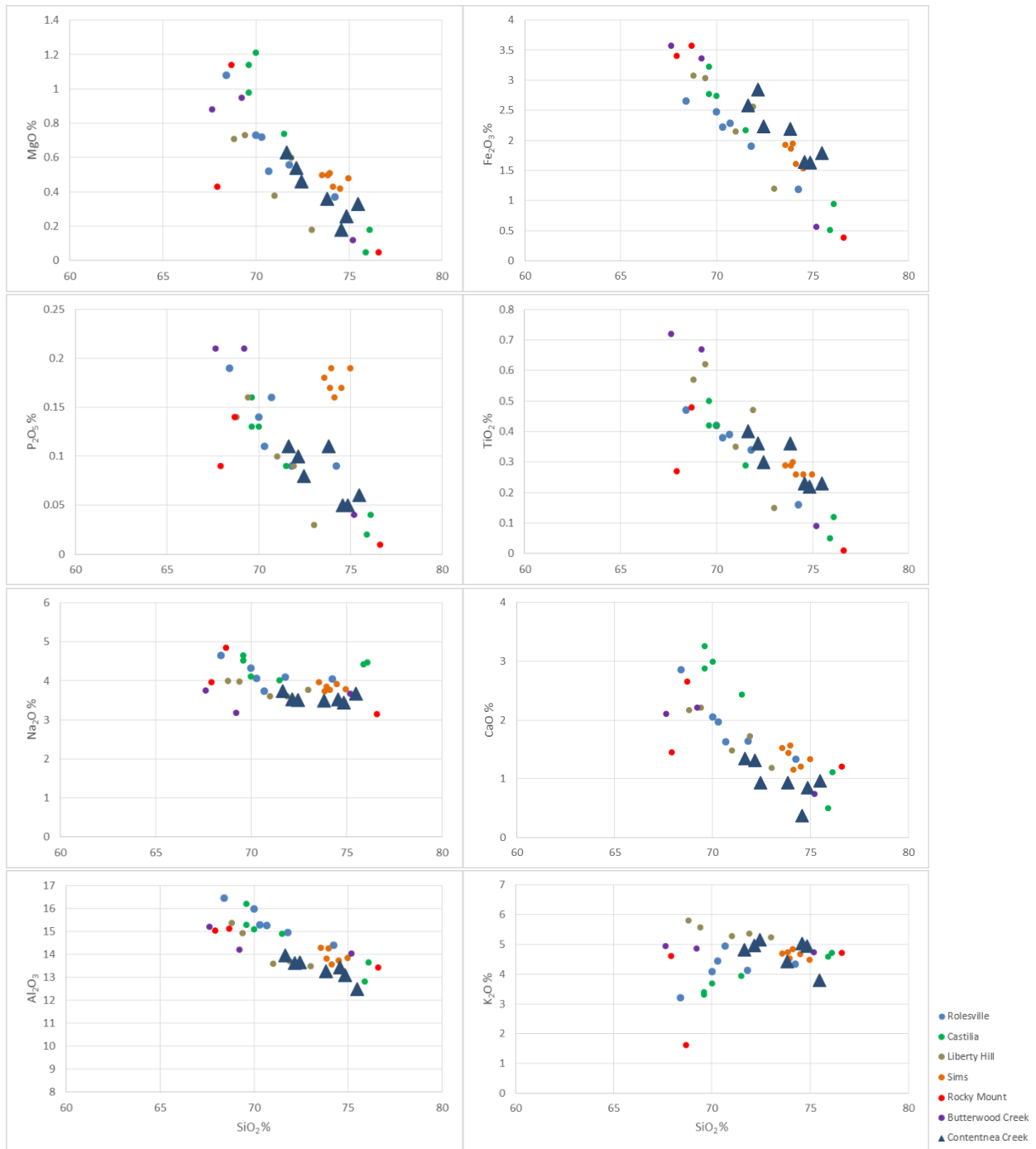
Figure 14. Major element (wt. %) versus SiO_2 (wt. %) diagrams. Data for Rolesville, Castilia, Liberty Hill, and Sims from Speer and Hoff (1997). Data for Rocky Mount and Butterwood Creek from Coler et al. (1997). Contentnea Creek data from this study.

The light rare earth element (LREE) concentrations for Alleghanian plutons generally show well-defined, linear decreases with increasing silica contents as well as a distinct negative Eu anomaly in chondrite-normalized REE patterns (Speer and Hoff, 1997), which is also the case with the Contentnea Creek pluton (Figure 15). Speer and Hoff (1997) concluded heavy rare earth element (HREE) concentrations for Alleghanian plutons show no obvious trend with increasing silica content, although there is little REE data for most Alleghanian plutons. The Contentnea Creek pluton does show a linear decrease in HREE with increasing SiO_2, however it is much less defined compared to the LREE (Figure 15). The chondrite-normalized REE patterns in the Contentnea Creek pluton are similar to the Alleghanian mean REE patterns (Figure 16). These patterns have fairly gentle slopes, are enriched in LREEs, and show low abundances of HREEs.
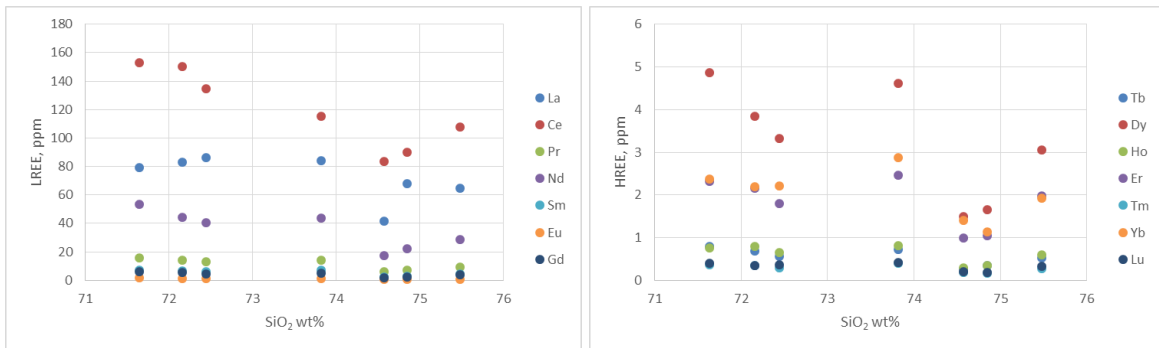
Figure 15. Rare earth elements (ppm) versus SiO_2 (wt. %) diagrams from the Contentnea Creek pluton.
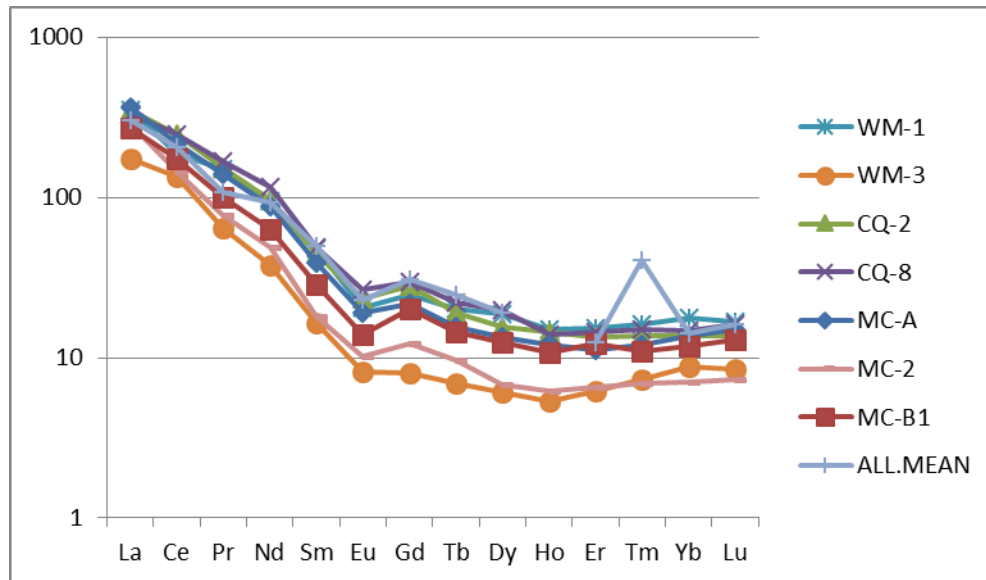
Figure 16. Rare earth element chondrite-normalized spider diagram for the Contentnea Creek pluton and the Alleghanian mean. Normalizing REE values from McDonough and Sun (1995).

3.5. Geochronology

Zircons are wide-spread minerals of great importance in investigations on the genesis, evolution, and age of rocks (Kober, 1987). They are prominent carriers of radioactivity as they strongly fractionate uranium (U) and thorium (Th) from lead (Pb) during their crystallization. Bulk samples from the Contentnea Creek pluton were mechanically disaggregated using a jaw crusher and disk mill. Zircon and other heavy minerals were isolated by their high densities using a water table. This heavy mineral mixture was separated using methylene-iodide (s.g. 3.32), in which minerals such as magnetite and zircon will sink, whereas quartz and feldspars will float. Magnetite grains and other magnetic minerals were removed from each sample using a hand magnet and a Frantz magnetic separator operated at 1.5 A and 10° side tilt. Individual zircon grains were selected using a binocular microscope. Selected grains were thermally annealed for 48 h at 900 °C and then chemically abraded for 12 h at 180 °C to remove inclusions and eliminate any volumes affected by radiation damage (Mattinson, 2005). Selected grains were

30

dissolved in 29 M HF acid and spiked using a ^{205}Pb-^{233}U-^{236}U tracer. Anion exchange (HCl) column chromatography was used to isolate U and Pb from the solution.

Isotopic ratios of both U and Pb were determined by thermal ionization mass spectrometry (TIMS) on a VG Sector 54 mass spectrometer at the University of North Carolina at Chapel Hill under the direction of Dr. Drew Coleman. Uranium was run on single Re filaments as an oxide (UO$_2$), after loading in silica gel. Lead was loaded in silica gel on single zone-refined Re filaments. All data was collected in single-collector peak-switching mode using the Daly ion-counting system. Data processing and age calculations were completed using Tripoli and U-Pb Redux developed as part of the EARTHTIME initiative. Decay constants used were ^{238}U = 0.155125 x 10^{-9} + 0.16598 x 10^{-14} a-1 and ^{235}U = 0.98485 x 10^{-9} + 0.13394 x 10^{-13} a-1. All errors are reported at 2-sigma uncertainty and considered analytical and decay-constant uncertainties.

Five zircons were analyzed from the eastern margin of the Contentnea Creek pluton. Most fractions from the sample are concordant within uncertainty after the application of a Th correction (Figure 17). Consequently, we report the weighted mean ^{206}Pb/^{238}U ages of the concordant samples as the best estimate for the crystallization age.
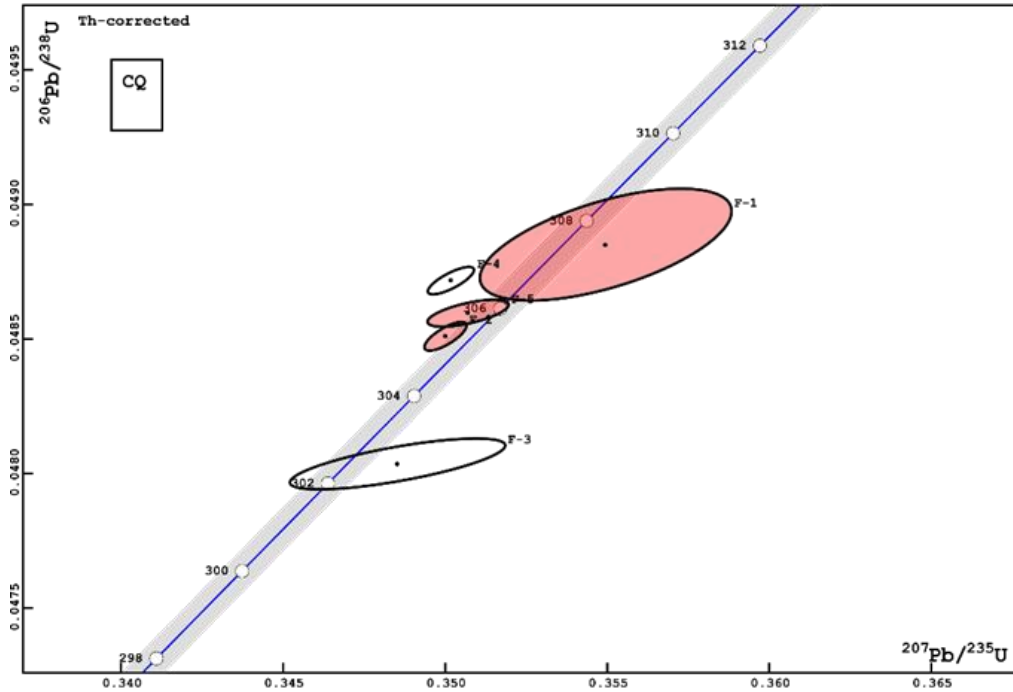
Figure 17. Conventional concordia diagram for fractions from the Contentnea Creek pluton. Black dots inside of ellipses represent weighted mean dates for each fractionation. Ellipses represent error. Ellipses highlighted in red are accepted fractions.

The first fraction (F-1) yields a $^{206}Pb/^{238}U$ age of 307.50 ± 1.3 Ma and is concordant within uncertainty. F-2 yields an age of 305.36 ± 0.33 Ma and is concordant within uncertainty. F-3 yields an age of 302.45 ± 0.58 Ma and is concordant within uncertainty. F-4 yields an age of 306.64 ± 0.31 Ma but is not concordant within uncertainty. F-5 yields an age of 305.89 ± 0.31 Ma and is concordant within uncertainty. F-3 and F-4 were excluded from the weighted mean $^{206}Pb/^{238}U$ ages due to their degree of discordance and uncertainty. Therefore, the weighted mean $^{206}Pb/^{238}U$ zircon age of 305.70 ± 0.22 Ma (MSWD = 6.7) is accepted as the crystallization age for the Contentnea Creek pluton, assuming it is a single pulse intrusion (Figure 18).
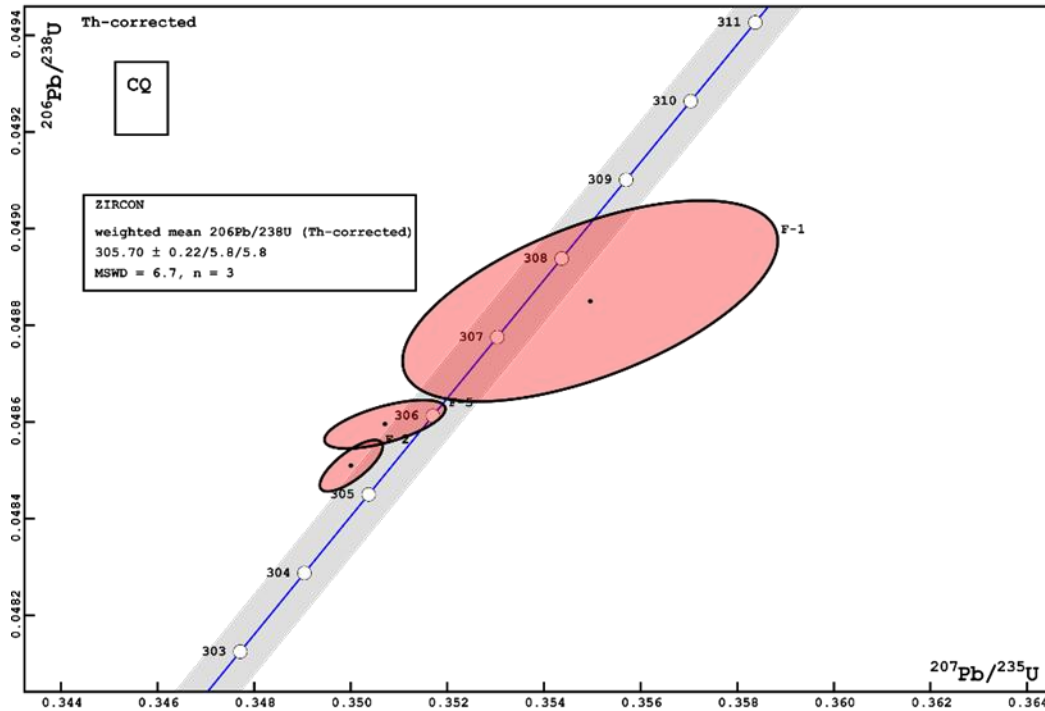
Figure 18. Conventional concordia diagram for accepted fractions from the Contentnea Creek pluton. Weighted mean[206]Pb/[238]U date for fractions is shown in the ellipses along concordia. Also shown is the mean square of weighted deviation (MSWD).

3.6. Paleostress Analysis

A shear fracture is a planar surface in which relative movement is parallel to the fracture (Fossen, 2010). Populations of shear fractures commonly form in preferred orientations in the shallow crust at low temperatures and pressures relative to a 3-D stress field. Due to physical abrasion during slip, lineations called slickenlines often form on shear fractures (Fossen, 2010). Using the slickenline directions and sense of motion on a fault surface, it is possible to reconstruct inferred stress tensors that correlate with the orientation of paleostress axes and the ratio between principal stress values (Angelier, 1984). Inferred stress tensors can be interpreted to test hypotheses about regional tectonics.

33

The orientations of 16 shear fractures and slickenlines were measured from the western margin of the pluton (Figure 19A, B). Shear fractures tend to be found in clusters and, from available exposure, decrease in abundance to the east (Figure 19C, D). Shear fracture orientations were input into the FaultKin program to calculate inferred paleostress axes (Figure 20).

Figure 19. Photographs of shear fractures from the western margin of the Contentnea Creek pluton. (A) Shows slickenside surface as well as slickenlines. (B) Two closely related shear fractures in different orientations labeled "sf". (C) A population of mineralized shear fractures. (D) A population of mineralized shear fractures high lighted by dashed white lines.

The results of paleostress analysis are plotted on equal angle, lower hemisphere stereographic projections in Figure 20. Shear fractures surfaces generally strike NE-SW with some in a N-S orientation and dip moderately to steeply N-NE-E-SE-S ranging from 36-88°. Slickenlines on the fault surfaces have relatively shallow to moderate plunges ranging from 0-

42° and generally trend to the southwest. Assuming right-lateral faulting, inferred maximum stress (σ_1) plunges shallowly to the northeast (07→030) while inferred intermediate (σ_2) and inferred minimum stresses (σ_3) plunge moderately to the southeast and northwest (49→128; 40→294), respectively (Figure 20A). Assuming left-lateral faulting inverts the orientation of the inferred maximum stress and the inferred minimum stress (Figure 20B).
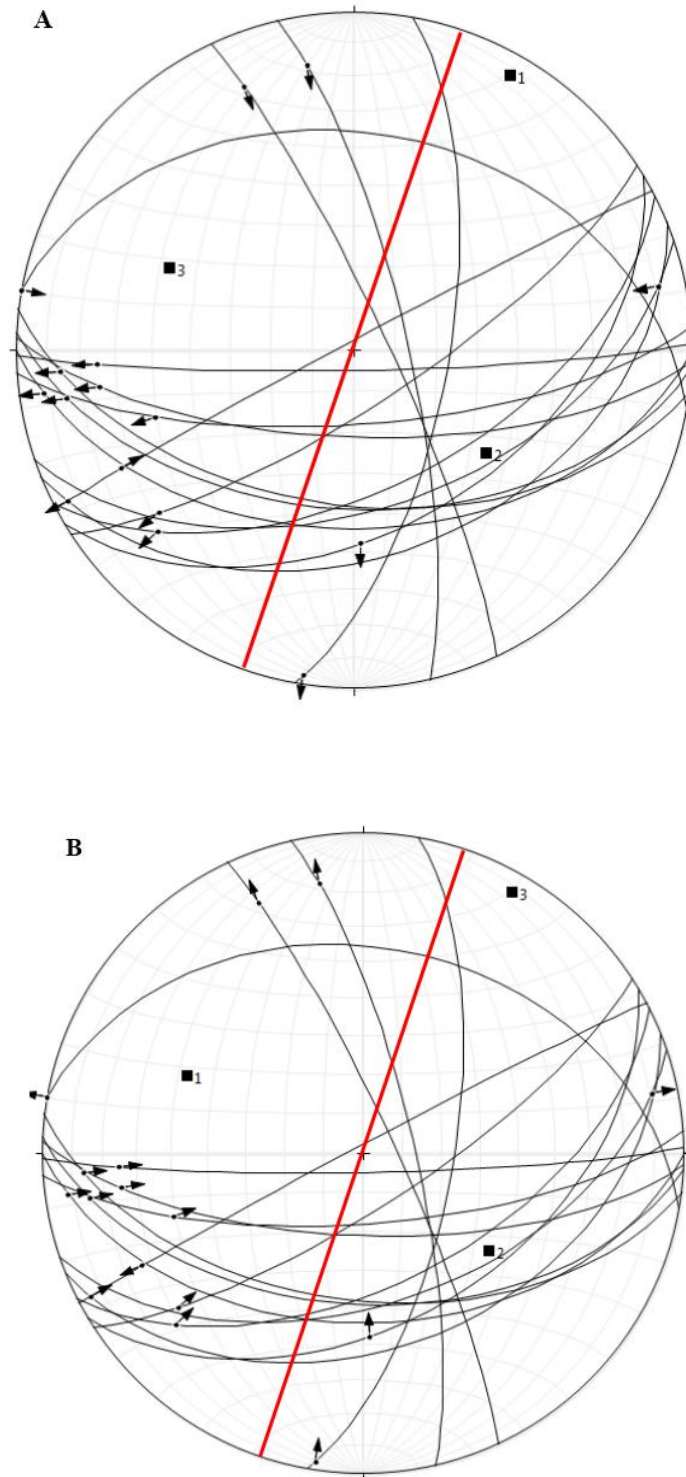
Figure 20. Lower hemisphere stereographic projection of paleostress analysis. Black arcs represent shear fracture surfaces, black dots represent striae lineations, black squares represent inferred stress axes (inferred $\sigma_1 = 1$, $\sigma_2 = 2$, $\sigma_3 = 3$). The red line represents the approximate orientation of the HMZ. (A) Inferred paleostress axes assuming all fractures are right-lateral. (B) Inferred paleostress axes assuming all fractures are left-lateral.

4. Discussion

4.1. Petrography

Petrographic analysis of the Contentnea Creek pluton demonstrates fabric variations that suggest different deformation histories between the western and eastern margin of the pluton. The eastern margin of the pluton, away from the fault zone, displays magmatic fabrics. The western margin of the pluton, close to the fault zone, displays HTSS fabric and cross-cutting LTSS fabric. The central portions of the pluton display HTSS fabric as well as possible locally developed LTSS fabric. However, the fairly undeformed nature of feldspar crystals and evidence of recrystallized quartz crystals could suggest the superposition of solid-state deformation on a magmatic foliation (Patterson et al., 1989). Fabrics from the western and central portions of the pluton suggest the HMZ was active during the emplacement.

4.2. Fabric Analysis

Two separate fabric analysis techniques were used to study the Contentnea Creek Pluton. SPO and AMS in granitic rocks are controlled by the shape fabric and spatial distribution of mineral grains. Although SPO samples are limited, the SPO results are important in understanding fabrics in the Contentnea Creek pluton and can be compared with other fabric techniques. Interpretations of magnetic fabrics require a detail knowledge of magnetic mineralogy. Loose constraints on magnetic mineralogy from petrology and bulk susceptibility are available for this study and suggest magnetite is the dominant cause of the AMS signal. Future study in this area should involve additional SPO analysis in the central portions of the pluton and more rigorous analysis of the magnetic mineralogy to allow for better interpretations.

The orientations of the principal axes are similar for both fabric techniques. However, the orientations of magnetic major and minor axes (K_1 and K_3) are inverted compared to the major

and minor axes from SPO. Inverse magnetic fabrics are consistent with single-domain magnetite. Single-domain magnetite grains have their long axes parallel to K_3, which is the short axis of the AMS tensor (Potter and Stephenson, 1988; Ferre, 2002). Therefore, inverse long and short axes are expected with contribution of single-domain magnetite grains to the low-field AMS signal.

Fabrics formed during tectonic processes record the interactions between local driving forces and regional tectonic forces. Shape parameters are dependent on the rheological conditions during formation and reflect information on the intensity and orientation of strain. The western margin and internal parts of the intrusion display mostly oblate fabrics, while the eastern margin displays mostly prolate fabrics. The oblate fabrics are consistent with transpression (Saint-Blanquat and Tikoff, 1997). Prolate fabrics are less consistent with transpression, but could be associated with local linear strain.

The western margin of the pluton displays solid-state fabrics. Assuming single-domain magnetite, fabric patterns observed from the western margin are similar in orientation to the nearby HMZ. The moderate-steeply dipping foliation and shallowly plunging lineation probably record strain that occurred while the HMZ was active and the pluton was cooling. The eastern margin of the pluton displays magmatic fabrics. Fabric patterns observed from the eastern margin are closely related to the orientation of the hypothesized boundary of the pluton. The subvertical foliation and lineation probably records strain that occurred during emplacement and were not greatly influenced by the nearby HMZ. Types of fabrics displayed in the central parts of the pluton are unclear. However, central parts closer to the HMZ display orientations similar to the western margin, while central parts away from the HMZ display more variable orientations. The change in fabric patterns suggest a different thermal and strain rate history between the parts of the pluton inside and outside the HMZ.

38

4.3. Geochemistry

The Contentnea Creek pluton is geochemically similar to other Alleghanian plutons in the southern Appalachians. Most major oxides display a linear decrease with increasing SiO_2. Trace elements and REEs also show a small linear decrease in abundance with increasing silica content. Chondrite-normalized REE patterns show gentle negative slopes with a small negative Eu anomaly, which could suggest prior fractionation of plagioclase (Speer and Hoff, 1997).

No chemical trends exist between different locations in the pluton or with distance from the HMZ. Present levels of exposure suggest the pluton is relatively small and probably assembled rapidly, so the lack of geochemical variation is not surprising.

4.4. Geochronology

Most zircon fractions from the geochronology study yield concordant data for which weighted mean $^{206}Pb/^{238}U$ ages are calculated. The mean weighted zircon U/Pb age of 305.70 ± 0.22 Ma is the accepted crystallization age of the Contentnea Creek pluton, assuming it is a single pulse intrusion. An Alleghanian thermal event affected rocks of the eastern Piedmont of North Carolina. The duration of the event is not known, however, it was associated with numerous Alleghanian granitic plutons. The 305 Ma age falls into the existing range of ages for other Alleghanian granites of the eastern North Carolina Piedmont.

Given the spatial and temporal relationship between the HMZ and the Contentnea Creek pluton, the age of crystallization helps constrain the Paleozoic slip history of the HMZ. Although it may have initiated earlier, HMZ movement occured between the time of intrusion of the Contentnea Creek pluton and regional cooling (250-240 Ma). Brittle structures within the intrusion indicate the HMZ was later reactivated, however this does not conflict with the HMZ having major Alleghanian movement.

4.5. Paleostress Analysis

Solid-state fabrics within the Contentnea Creek pluton suggest the intrusion was deformed by the HMZ under different conditions, an early high-temperature event and a later low-temperature event. A population of striae and minor brittle faults in the Contentnea Creek pluton record a similar sense of slip as ductile structures in other locations along the HMZ. These relationships indicate some parts of the HMZ underwent ductile shearing as well as brittle faulting, suggesting the HMZ may have been reactivated. Differential uplift in the Alleghanian due to post-metamorphic cooling may have been accommodated by movement along ductile shear zones (Stoddard et al., 1991), possibly causing brittle faulting along the HMZ. However, Cretaceous and Cenozoic faults have been recognized in the eastern Piedmont of North Carolina (e.g. Prowell, 1983). Ongoing regional compressive stresses from the east-northeast and west-southwest are similar to both inferred maximum stress orientations, suggesting shear fractures in the Contentnea Creek pluton may have formed in the late Cenozoic stress field.

5. Conclusions

During the Alleghanian orogeny, the Contentnea Creek pluton was affected by the HMZ. The eastern margin of the pluton displays magmatic fabrics consistent with slow cooling and low strain rates. The western margin of the pluton displays high-temperature solid-state fabrics locally overprinted by low-temperature solid-state fabrics and isolated clusters of mineralized shear fractures. The central portions of the pluton are texturally different from the pluton margins and show evidence of local high-temperature solid-state deformation superimposed on magmatic fabrics.

The Contentnea Creek pluton is relatively small and is geochemically homogenous within the exposed area. The intrusion is geochemically similar to other Alleghanian grantoids in the southern Appalachians and likely originated from a similar source. The 305.70 ± 0.22 Ma crystallization age falls within the range of other plutons in the eastern Piedmont of North Carolina including those along the HMZ. Although the HMZ may have had an earlier slip history and was possibly later brittely reactivated, these new structural and geochronological data demonstrate the structure was active during emplacement of the Contentnea Creek pluton.

Mineralized shear fractures in the Contentnea Creek pluton overprint late Paleozoic Alleghanian structures. Other brittle deformation overprinting similar late Paleozoic structures has been recognized in Virginia, Georgia, and South Carolina. The timing of late brittle structures in the Contentnea Creek pluton is unclear, however inferred paleostress directions are consistent with previous estimates of the Holocene regional stress field and suggest late Cenozoic reactivation of the HMZ.

REFERENCES

Ando, C.J., Czuchra, B.L., Klemperer, S.L., Brown, L.D., Cheadle, M.J., Cook, F.A, Oliver, J.E., Kaufman, S., Walsh, T., Thompson Jr., J.B., Lyons, J.B., Rosenfeld, J.L., 1984. Crustal profile of a mountain belt: COCORP deep seismic reflection profiling in New England Appalachians and implications for architecture of convergent mountain chains. American Association of Petroleum Geologist Bulletin 68, 819-837.

Bobyarchick, A.R., 1981. The Eastern Piedmont Fault System and Its Relationship to Alleghanian Tectonics in the Southern Appalachians. Journal of Geology 89, 335-347.

Bouchez, J.L., 1997. Granite is never isotropic: An introduction to AMS studies of granitic rocks. In: Bouchez, J. L., Hutton, D. H. W., Stephens, W. E. (Eds.), Granite: from Segregation of Melt to Emplacement Fabrics. Kluwer, Dordrecht, 95-112.

Burns, R.W., Horsman, E.M., 2013. Tectonic evolution of the Contentnea Creek Pluton, eastern Piedmont, Wilson County, North Carolina. Undergraduate Research & Creative Achievement Week, East Carolina University, Poster.

Coler, D.G., Samson, S.D., Speer, J.A., 1997. Nd and Sr isotopic constraints on the source of Alleghanian granites in the Raleigh metamorphic belt and Eastern slate belt, southern Appalachians. U.S.A. Chemical Geology 134, 257-275.

Drake Jr., A.A., Sinha, A.K., Laird, J., Guy, R.E., 1989. The Taconic orogeny. In: Hatcher Jr., R.D., Thomas, W.A., Viele, G.W. (Eds.), The Appalachian-Ouachita Orogen in the United States: Boulder, Colorado, Geological Society of America, The Geology of North America F-2, 101-177.

Farrar, S.S., 1985a. Stratigraphy of the northeastern North Carolina Piedmont. Southeastern Geology 25, 159-183.

Farrar, S.S., 1985b. Tectonic evolution of the easternmost Piedmont, North Carolina. Geological Society of America Bulletin 96, 362-380.

Ferre, E.C., 2002. Theoretical models of intermediate and inverse AMS fabrics. Geophysical Research Letters 29, 1127.

Fletcher, C.D., 1992. A Geophysical study of the Hollister mylonite zone, Northeastern North Carolina. Master's Thesis. Department of Geological Sciences. East Carolina University.

Fossen, H., 2010. Structural Geology: Cambridge University Press, 124.

Fullagar, P.D., Butler, J.R., 1979. 325 to 265 m.y.-old granitic plutons in the piedmont of the southern Appalachians. American Journal of Science 279, 161-185.

Glover, L. III, Speer, J.A., Russell, G.S., Farrar, S.S., 1983. Ages of regional metamorphism and ductile deformation in the central and southern Appalachians. Lithos 16, 233-245.

Hatcher Jr., R.D., Howell, D.E., Talwani, P., 1977. Eastern Piedmont Fault system: Speculations on its extent. Geology 5, 636-640.

Hatcher Jr., R.D., Thomas, W.A., Geiser, P.A., Snoke, A.W., Mosher, S., Wiltschko, D.V., 1989. Alleghanian orogeny. In: Hatcher Jr., R.D., Thomas, W.A., Viele, G.W. (Eds.), The Appalachian-Ouachita Orogen in the United States: Boulder, Colorado, Geological Society of America, The Geology of North America F-2, 233-318.

Hatcher Jr., R.D., 2010. The Appalachian orogen: A brief summary. Geological Society of America Memoir 206, 1-19.

Horsman, E., Tikoff, B., Sven, M., 2005. Emplacement-related fabric and multiple sheets in the Maiden Creek sill, Henry Mountains, Utah, USA. Journal of Structural Geology 27, 1426-1444.

Kober, B., 1987. Single-zircon evaporation combined with Pb^+ emitter bedding for $^{207}Pb/^{206}Pb$-age investigation using thermal ion mass spectrometry, and implication to zirconology. Contributions to Mineralogy and Petrology 96, 63-71.

Launeau, P., Bouchez, J.L., Benn, K., 1990. Shape preferred orientation of object populations: automatic analysis of digitized images. Tectonophysics 180, 201-211.

Launeau, P., Cruden, A.R., 1998. Magmatic fabric acquisition mechanisms in a syenite: Results of a combined anisotropy of magnetic susceptibility and image analysis study. Journal of Geophysical Research 103, 5067-5089.

Launeau, P., Robin, P.Y., 2005. Determination of fabric and strain ellipsoids from measured sectional ellipses - implementation and application. Journal of Structural Geology 27, 2223-2233.

Launeau, P., Archanjo, C.J., Picard, D., Arbaret, L., Robin, P.Y., 2010. Two- and three-dimensional shape fabric analysis by the intercept method in grey levels. Tectonophysics 492, 230-239.

Lawrence, D.P., 1999. Bouguer gravity study along the Hollister Fault Zone, Eastern North Carolina. Carolina Geological Society Guidebook, 37-48.

Marple, R.T., Talwani, P., 2000. Evidence for a buried fault system in the Coastal Plain of the Carolinas and Virginia - Implications for neotectonics in the southeastern United States. GSA Bulletin 112, 200-220.

Mattinson, J.M., 2005. Zircon U-Pb chemical abrasion ("CA-TIMS") method: Combined annealing and multi-step partial dissolution analysis for improved precision and accuracy of zircon ages. Chemical Geology 220, 47-66.

McDonough, W.F., Sun, S.S., 1995. The composition of the Earth. Chemical Geology 120, 223-253.

Moncla, A.M., 1990. Petrography, Geochemistry, and Geochronology of the Rocky Mount Batholith, Northeastern North Carolina Piedmont. Master's Thesis. Department of Geological Sciences. East Carolina University.

Montaser, A., 1998. Inductively coupled plasma mass spectrometry: New York, Wiley, 967.

Osberg, P.H., Tull, J.F., Robinson, P., Butler, J.R., 1989. The Acaidan orogeny. In: Hatcher Jr., R.D., Thomas, W.A., Viele, G.W. (Eds.), The Appalachian-Ouachita Orogen in the United States: Boulder, Colorado, Geological Society of America, The Geology of North America F-2, 179-232.

Paterson, S.R., Vernon, R.H., Tobisch, O.T., 1989. A review of criteria for the identification of magmatic and tectonic foliations in granitoids. Journal of Structural Geology 11, 349-363.

Potter, D.K., Stephenson, A., 1988. Single-domain particles in rocks and magnetic fabric analysis. Geophysical Research Letters 15, 1097-1100.

Prowell, D.G., 1983. Index faults of Cretaceous and Cenozoic age in the Eastern United States. U.S. Geological Survey Miscellaneous Field Studies Map MF-1269.

Rochette, P., Jackson, M., Aubourg, C., 1992. Rock magnetism and the interpretation of anisotropy of magnetic susceptibility. American Geophysical Union 30, 209-226.

Russell, G.S., Russell, C.W., Farrar, S.S., 1985. Alleghanian deformation and metamorphism in the eastern North Carolina Piedmont. Geological Society of America Bulletin 96, 381-387.

Sacks, P.E., 1999. Geologic Overview of the Eastern Appalachian Piedmont Along Lake
        Gaston, North Carolina and Virginia. Carolina Geological Society Guidebook, 1-14.

Saint-Blanquat, M., Tikoff, B., 1997. Development of magmatic to solid-state fabrics during
        syntectonic emplacement of the Mono Creek Granite, Sierra Nevada Batholith. In:
        Granite: From segregation of melt to emplacement fabrics, Petrology and structural
        geology 8, 231-252.

Secor Jr., D.T., Samson, S.L., Snoke, A.W., Palmer, A.R., 1983. Confirmation of the
        Carolina Slate Belt as an exotic terrane. Science 221, 649-651.

Snoke, A.W., Kish, S.A., Secor Jr., D. T., 1980. Deformed Hercynian granitic rocks from
        the Piedmont of South Carolina. American Journal of Science 280, 1018-1034.

Speer, J.A., Hoff, K., 1997. Elemental composition of the Alleghanian granitoid plutons of the
        southern Appalachians. Geological Society of America Bulletin 191, 287-308.

Speer, J.A., McSween Jr., H.Y., Gates, A. E., 1994. Generation, Segregation, Ascent, and
        Emplacement of Alleghanian Plutons in the Southern Appalachians. The Journal of
        Geology 102, 249-267.

Stoddard, E.F., Farrar, S.S., Horton Jr., J.W., Butler, J.R., Drunhan, R.M., 1991. The Eastern
        Piedmont in North Carolina: In. The Geology of the Carolinas, 79-92.

Tomezzoli, R.N., MacDonald, W.D., Tickyj, H., 2003. Composite magnetic fabrics and S-C
        structure in granitic gneiss of Cerro de los Viejos, La Pampa Province, Argentina. Journal
        of Structural Geology 25, 159-169.

Vyhnal, C.R., McSween Jr., H. Y., 1990. Constraints on Alleghanian vertical crustal
        displacements in the southern Appalachians, based on aluminum-hornblende
        barometry. Geology 18, 938-941.

Vyhnal, C.R., McSween Jr., H.Y., Speer, J.A., 1991. Hornblende chemistry in southern
        Appalachian granitoids: Implications for aluminum hornblende thermobarometry and
        magmatic epidote stability. American Mineralogist 76, 176-188.

Wedemeyer, R.G., Spruill, R.K., 1980. Geochemistry and geochronology of the Sims granite,
        eastern Carolina slate belt, North Carolina. Geological Society of America Abstracts with
        Programs 12, 211.

Wilson, W.E., 1979. Geology of Wilson County, NC. North Carolina Department of Natural
        Resources and Community Development, Division of Land Resources, Geological
        Survey Section.

Appendix A   AMS Data

Name	K1	K2	K3	K1dec	K1inc	K2dec	K2inc	K3dec	K3inc
OW-A1-A1	1.0714	1.0061	0.9225	234.2	34.2	108.4	40.8	347.8	30.5
OW-A1-A2	1.0676	1.0110	0.9214	217.3	33.3	95.2	39.0	333.0	33.4
OW-A2-A1	1.0648	1.0089	0.9263	247.5	47.3	98.7	38.3	355.6	16.0
OW-A2-A2	1.0439	1.0093	0.9468	230.2	42.4	90.7	39.8	341.4	21.6
OW-A2-A3	1.0383	1.0222	0.9396	233.0	25.3	90.7	59.2	331.0	16.4
MC-A3-A1	1.1032	0.9813	0.9155	227.8	53.1	338.1	14.7	77.9	33.0
MC-A3-A2	1.0780	1.0081	0.9139	215.5	39.4	322.3	19.4	72.4	44.3
MC-A1-A1	1.0671	1.0102	0.9228	219.8	57.4	322.6	8.1	57.5	31.3
MC-A1-A2	1.0680	0.9901	0.9419	228.9	53.7	332.0	9.4	68.6	34.7
MC-A1-A3	1.0804	0.9993	0.9203	197.3	57.2	314.8	16.6	53.7	27.4
MC-A2-A1	1.0964	0.9880	0.9156	205.1	50.4	328.1	24.3	72.7	29.2
MC-A2-A2	1.0909	1.0162	0.8929	216.8	52.9	322.7	11.7	60.9	34.6
MC-A4-A1	1.0958	0.9871	0.9171	218.6	20.0	315.1	17.4	83.0	63.0
MC-A5-A1	1.0900	1.0050	0.9050	217.4	60.1	324.2	9.4	59.3	28.1
MC2-A1	1.0909	1.0374	0.8717	150.6	2.1	241.6	24.3	55.9	65.6
MC2-A2	1.0922	1.0611	0.8466	312.6	2.3	221.6	23.7	47.9	66.2
MC2-A3	1.0860	1.0401	0.8738	155.0	7.5	247.8	20.2	45.8	68.4
MC-B1-A1	1.0617	1.0007	0.9376	303.6	38.8	195.9	20.7	84.5	43.9
MC-B1-A2	1.0688	1.0150	0.9162	275.4	46.7	179.3	5.7	84.1	42.7
MC-B1-A3	1.0624	1.0183	0.9193	296.9	48.7	188.3	15.6	86.1	37.0
MC-B2-A1	1.0497	1.0057	0.9446	118.8	72.4	324.2	16.0	232.1	7.2
MC-B2-A2	1.0451	1.0057	0.9492	118.2	50.2	327.0	36.2	226.2	14.4
MC-B3-A1	1.0549	1.0041	0.9410	91.3	44.7	307.9	39.1	201.4	19.2
MC-B4-A1	1.0366	1.0303	0.9331	74.8	50.0	299.2	30.9	194.7	22.7
OC-A1-A1	1.0691	0.9904	0.9405	217.2	9.1	312.0	27.3	110.5	61.0
OC-A1-A2	1.0425	1.0222	0.9353	220.1	14.1	319.5	33.1	110.4	53.3
OC-A1-A3	1.0707	0.9673	0.9619	218.6	11.4	123.9	22.1	334.1	64.8
OC-A2-A1	1.0710	0.9891	0.9399	35.20	11.9	292.1	47.1	135.5	40.5
OC-A2-A2	1.0703	0.9900	0.9397	228.2	5.9	321.2	26.5	126.8	62.7
OC-A2-A3	1.0743	0.9880	0.9377	33.3	9.2	294.2	44.0	132.4	44.5
Average	1.0701	1.0069	0.9230	198.6	35.1	253.3	26.0	150.8	38.6

AMS data, continued

Name	Km µSI	L	F	Pj	T
OW-A1-A1	4085.127	1.065	1.091	1.162	0.160
OW-A1-A2	2428.122	1.056	1.097	1.161	0.260
OW-A2-A1	1572.667	1.055	1.089	1.151	0.226
OW-A2-A2	753.890	1.034	1.066	1.104	0.310
OW-A2-A3	1031.587	1.016	1.088	1.113	0.687
MC-A3-A1	25867.510	1.124	1.072	1.208	-0.255
MC-A3-A2	21548.110	1.069	1.103	1.181	0.188
MC-A1-A1	10656.250	1.056	1.095	1.158	0.246
MC-A1-A2	17866.970	1.079	1.051	1.135	-0.205
MC-A1-A3	20744.210	1.081	1.086	1.174	0.026
MC-A2-A1	16506.460	1.110	1.079	1.198	-0.155
MC-A2-A2	19290.710	1.074	1.138	1.225	0.291
MC-A4-A1	30549.520	1.110	1.076	1.196	-0.174
MC-A5-A1	24260.520	1.085	1.110	1.205	0.126
MC2-A1	11244.250	1.052	1.190	1.265	0.551
MC2-A2	14232.580	1.029	1.253	1.322	0.773
MC2-A3	12429.030	1.044	1.190	1.259	0.603
MC-B1-A1	9827.494	1.061	1.067	1.132	0.048
MC-B1-A2	11272.290	1.053	1.108	1.170	0.330
MC-B1-A3	9827.626	1.043	1.108	1.160	0.413
MC-B2-A1	8185.960	1.044	1.065	1.112	0.187
MC-B2-A2	12935.850	1.039	1.060	1.102	0.202
MC-B3-A1	10404.350	1.051	1.067	1.121	0.136
MC-B4-A1	8526.919	1.006	1.104	1.125	0.885
OC-A1-A1	30921.860	1.079	1.053	1.138	-0.193
OC-A1-A2	29257.440	1.020	1.093	1.123	0.637
OC-A1-A3	28772.470	1.107	1.006	1.128	-0.896
OC-A2-A1	23652.090	1.083	1.052	1.141	-0.219
OC-A2-A2	25183.330	1.081	1.054	1.140	-0.198
OC-A2-A3	21127.740	1.087	1.054	1.147	-0.232
Average	15498.764	1.063	1.092	1.165	0.159

Appendix B   Geochemistry Data

Whole-rock major element geochemistry data

Major element (wt%)								
	WM-1	**WM-3**	**MC-A**	**MC-2**	**MC-B1**	**CQ-2**	**CQ-8**	
								AVG
SiO_2	73.82	74.57	72.44	74.85	75.48	72.16	71.64	73.57
Al_2O_3	13.25	13.43	13.66	13.09	12.49	13.62	13.96	13.36
TiO_2	0.36	0.23	0.30	0.22	0.23	0.36	0.40	0.30
Fe_2O_3	2.19	1.64	2.23	1.63	1.79	2.84	2.58	2.13
MnO	0.04	0.02	0.08	0.02	0.06	0.05	0.05	0.05
MgO	0.36	0.18	0.46	0.26	0.33	0.54	0.63	0.39
CaO	0.93	0.37	0.93	0.85	0.96	1.31	1.35	0.96
Na_2O	3.49	3.52	3.51	3.45	3.67	3.52	3.74	3.56
K_2O	4.43	5.04	5.16	4.94	3.79	4.97	4.81	4.73
P_2O_5	0.11	0.05	0.08	0.05	0.06	0.10	0.11	0.08
LOI	0.80	0.80	0.90	0.50	1.00	0.30	0.50	0.69
Sum	99.81	99.86	99.79	99.86	99.88	99.78	99.77	99.82

Whole-rock trace element geochemistry data

	CQ-2	CQ-8	MC-A	MC-B1	MC-2	WM-1	WM-3	
Trace element (ppm)								**AVG**
Ba	741	805	930	354	584	652	533	657
Be	<1	2	4	3	4	5	7	4
Co	2.3	3.0	5.2	3.7	2.2	2.4	1.5	2.9
Cs	2.0	2.2	2.5	1.7	1.4	1.5	3.0	2.0
Ga	16.9	18.8	18.4	16.0	14.0	18.5	18.4	17.3
Hf	6.3	6.6	6.3	4.3	3.5	6.7	5.0	5.5
Nb	28.1	33.2	29.3	27.4	14.9	34.1	28.0	27.8
Rb	169.3	183.6	197.3	153.5	157.0	171.5	217.7	178.6
Sn	2	3	2	1	<1	2	1	2
Sr	298.4	354.5	293.8	235.1	315.1	328.5	212.4	291.1
Ta	2.6	2.7	2.9	2.3	1.0	3.1	2.5	2.4
Th	56.6	38.3	48.0	38.7	41.8	44.2	40.3	43.9
U	5.7	4.7	12.1	9.9	7.9	5.6	13.8	8.5
V	24	25	20	18	15	25	14	20
W	<0.5	<0.5	<0.5	<0.5	<0.5	0.70	<0.5	0.70
Zr	229.1	221.8	219.0	141.3	120.0	222.9	161.5	187.9
Y	23.0	25.5	18.5	17.4	9.1	24.3	9.6	18.2
La	82.9	79.0	86.4	64.8	68.0	84.1	41.3	72.4
Ce	150.5	152.7	134.5	107.8	89.8	115.0	83.3	119.1
Pr	14.18	15.49	12.99	9.36	7.23	14.09	5.95	11.33
Nd	44.3	53.5	40.5	28.7	22.2	43.8	17.2	35.7
Sm	6.58	7.26	5.78	4.28	2.68	7.05	2.45	5.15
Eu	1.31	1.49	1.08	0.79	0.57	1.16	0.46	0.98
Gd	5.59	5.92	4.35	4.03	2.43	4.92	1.61	4.12
Tb	0.69	0.80	0.56	0.52	0.35	0.73	0.25	0.56
Dy	3.84	4.86	3.32	3.05	1.66	4.62	1.49	3.26
Ho	0.79	0.76	0.66	0.59	0.34	0.82	0.29	0.61
Er	2.15	2.32	1.79	1.97	1.05	2.46	0.99	1.82
Tm	0.34	0.37	0.30	0.27	0.17	0.40	0.18	0.29
Yb	2.20	2.38	2.22	1.92	1.14	2.87	1.41	2.02
Lu	0.34	0.40	0.37	0.32	0.18	0.41	0.21	0.32
TOT/C	0.03	0.03	<0.02	0.08	<0.02	<0.02	<0.02	0.05
TOT/S	<0.02	<0.02	<0.02	<0.02	<0.02	<0.02	<0.02	<0.02
Mo	1.4	0.6	1.2	5.3	1.1	0.6	0.3	1.5
Cu	6.9	5.4	5.4	2.7	2.2	1.4	0.8	3.5
Pb	4.8	4.7	8.0	7.2	10.8	5.0	5.7	6.6
Zn	51	46	44	32	20	26	14	33
Ni	3.6	3.2	4.3	6.3	2.6	2.8	1.4	3.5
As	<0.5	<0.5	<0.5	<0.5	<0.5	<0.5	<0.5	<0.5
Cd	<0.1	<0.1	<0.1	<0.1	<0.1	<0.1	<0.1	<0.1

Whole-rock trace element geochemistry data, continued

Sb	<0.1	<0.1	<0.1	<0.1	<0.1	<0.1	<0.1	<0.1
Bi	<0.1	<0.1	<0.1	<0.1	<0.1	<0.1	0.20	0.20
Ag	<0.1	<0.1	<0.1	<0.1	<0.1	<0.1	<0.1	<0.1
Au (ppb)	1.1	0.6	<0.5	<0.5	0.7	<0.5	<0.5	0.8
Hg	<0.01	<0.01	<0.01	<0.01	<0.01	<0.01	<0.01	<0.01
Tl	0.1	0.1	0.1	<0.1	<0.1	<0.1	<0.1	0.1
Se	<0.5	<0.5	<0.5	<0.5	<0.5	<0.5	<0.5	<0.5
Ni	<20	<20	<20	<20	<20	<20	<20	<20
Sc	3	3	4	3	2	4	4	3

Appendix C　　　　　　**Geochronology Data**

Sample CQ Fraction	206Pb/238U \<Th\>a	2σ abs ±	207Pb/235 U b	2σ abs ±	207/206Pb b	2σ abs ±	Corr. Coef.	% disc. C
F-1	307.50	1.30	308.40	2.90	317.0	21	0.597	2.89
F-2	305.36	0.33	304.73	0.49	300.5	2.9	0.754	-1.58
F-3	302.45	0.58	303.60	2.50	313.0	19	0.729	3.48
F-4	306.64	0.31	304.86	0.53	291.9	3.2	0.779	-5.02
F-5	305.89	0.31	305.25	0.94	301.0	6.9	0.634	-1.58

Geochronology data, continued

	Conc U (ppm)	Th/U d	Pb (pg)	Pbc (Pg)	Pb/Pbc	206/204Pb	206Pb/ 238U	2σ % ±
F-1	353	0.77	52.1	1.70	31	1771	0.04884	0.43
F-2	754	0.63	636	1.85	343	20282	0.048495	0.11
F-3	910	0.71	81.5	2.67	31	1788	0.048021	0.20
F-4	653	0.74	891	3.91	228	13116	0.048702	0.10
F-5	821	0.68	384	6.45	59	3491	0.048581	0.10

Geochronology data, continued

	207Pb/235U	2σ % ±	207Pb/206Pb	2σ % ±	Corr. Coef.
F-1	0.35500	1.10	0.052710	0.91	0.597
F-2	0.35001	0.19	0.052346	0.12	0.754
F-3	0.34850	0.95	0.052640	0.82	0.729
F-4	0.35018	0.20	0.052148	0.14	0.779
F-5	0.35070	0.36	0.052360	0.30	0.634

Appendix D   **Paleostress Analysis Data**

Assumed Right-Lateral							Inferred **Paleostress axes**			
Number	Strike	Dip	Striae Trend	Plunge	Slip	T Trend	Plunge	P Trend	Plunge
1	90	46	262	8	NR	49	23	301	36
2	68	39	242	5	NR	31	29	276	38
3	92	69	262	25	NR	221	3	313	34
4	59	46	178	42	NR	344	1	250	75
5	86	72	251	38	NR	210	13	311	41
6	71	51	78	9	TR	37	34	294	20
7	93	51	260	15	NR	47	15	304	39
8	97	52	266	14	NR	51	15	309	37
9	347	77	351	16	TR	303	21	34	2
10	63	56	227	22	NR	13	7	276	41
11	57	76	230	26	NR	187	8	281	29
12	10	67	189	3	NR	327	14	232	18
13	242	88	243	24	TR	195	18	290	15
14	89	85	267	25	NR	220	14	316	21
15	280	36	280	0	TR	250	35	130	35
16	335	82	337	17	TR	290	18	22	6
NR= normal and right components							Mean Inferred Paleostress axes		
TR= thrust and right components							Eigenvalue	Trend	Plunge
						Axis 1	0.2266	29.7	7.1
						Axis 2	0.0029	128.0	49.0
						Axis 3	0.2296	293.7	40.1

Paleostress analysis data, continued

Assumed Left-Lateral							Inferred Paleostress axes			
Number	Strike	Dip	Striae Trend	Plunge	Slip	T Trend	Plunge	P Trend	Plunge
1	90	46	262	8	TL	301	36	49	23
2	68	39	242	5	TL	276	38	31	29
3	92	69	262	25	TL	313	34	221	3
4	59	46	178	42	TL	250	75	344	1
5	86	72	251	38	TL	311	41	210	13
6	71	51	78	9	NL	294	20	37	34
7	93	51	260	15	TL	304	39	47	15
8	97	52	266	14	TL	309	37	51	15
9	347	77	351	16	NL	34	2	303	21
10	63	56	227	22	TL	276	41	13	7
11	57	76	230	26	TL	281	29	187	8
12	10	67	189	3	TL	232	18	327	14
13	242	88	243	24	NL	290	15	195	18
14	89	85	267	25	TL	316	21	220	14
15	280	36	280	0	NL	130	35	250	35
16	335	82	337	17	NL	22	6	290	18
NL= normal and left components							Mean Inferred Paleostress axes			
TL= thrust and left components							Eigenvalue	Trend	Plunge	
						Axis 1	0.2296	293.7	40.1	
						Axis 2	0.0029	128.0	49.0	
						Axis 3	0.2266	29.7	7.1	